Semiannual Progress Report

For Stimul-Responsive Polymers with Enhanced Efficiency in Reservoir Recovery Processes

For the work performed during the period of

September 1, 2003 through February 29, 2004

by

Charles McCormick

and

Roger Hester

Issued on March 26, 2004

DOE Award Number DE-FC26-01BC15317

The University of Southern Mississippi
Department of Polymer Science
P.O. Box 10076
Hattiesburg, MS 39406

TABLE OF CONTENTS

LIST OF FIGURES AND TABLES

Disclaimer

Abstract

This report contains a series of terpolymers containing acrylic acid, methacrylamide and a twin-tailed hydrophobic monomer that were synthesized using micellar polymerization methods. These polymer systems were characterized using light scattering, viscometry, and fluorescence methods. Viscosity studies indicate that increasing the nonpolar character of the hydrophobic monomer (longer chain length or twin tailed vs. single tailed) results in enhanced viscosity in aqueous solutions. The interactions of these polymers with surfactants were investigated. These surfactants include sodium dodecyl sulfate (SDS), cetyl trimethylammonium bromide (CTAB), Triton X-100. Viscosity measurements of DiC_6AM and DiC_8AM mixtures indicate little interaction with SDS, gelation with CTAB, and hemimicelle formation followed by polymer hydrophobe solubilization with Triton X-100. The $DiC_{10}Am$ terpolymer shows similar interaction behavior with CTAB and Triton X-100. However, the enhanced hydrophobic nature of the DiC_{10} polymer allows complex formation with SDS as confirmed by surface tensiometry. Fluorescence measurements performed on a dansyl labeled $DiC_{10}Am$ terpolymer in the presence of increasing amounts of each of the surfactant indicate relative interaction strengths to be CTAB>Triton X-100>SDS.

A modified model based on Yamakawa-Fujii and Odjik-Skolnick-Fixman theories was found to describe the contribution of electrostatic forces to the excluded volume of a polyelectrolyte in solution. The model was found to be valid for flexible polymer coils in aqueous salt solutions where intermolecular interactions are minimal. The model suggested that a dimensionless group of parameters termed the dimensionless viscosity should be proportional to the dimensionless ratio of solution screening length to polyion charge spacing. Several sets of experimental data from the literature and from our laboratory have been analyzed according to the model and the results suggest that the two dimensionless groups are indeed related by a universal constant. This model has identified the parameters that are important to fluid mobility, thereby revealing methods to enhance solution performance when using polyions solutions as displacing fluids in oil reservoirs.

EXECUTIVE SUMMARY

To date, our synthetic research efforts have been focused on the development of stimuli-responsive water-soluble polymers designed for use in enhanced oil recovery (EOR) applications. These model systems are structurally tailored for potential application as viscosifiers and/or mobility control agents for secondary and tertiary EOR methods. The goal of previous synthetic work has been to design novel polymers that exhibit large dilute solution viscosities in the presence of the adverse conditions normally encountered in oil reservoirs (such as high salt concentrations, the presence of multivalent ions, and elevated temperatures). The polymers are also designed to have "triggerable" properties that can be elicited by external stimuli, such as changes in pH and/or salt concentration.

Previously, we have investigated polyzwitterions (i.e. polyampholytes and polybetaines) and hydrophobically modified polyelectrolytes as potential viscosifiers for EOR applications. The polyzwitterions demonstrate remarkable salt tolerance due to their amphoteric nature, while the hydrophobically modified (HM) polyelectrolytes exhibit improved viscosification as a result of intermolecular hydrophobic association, which imparts an additional viscosification mechanism to the polymers. This current research is focused on combining the benefits of polyzwitterions and hydrophobic modification in the same polymer system. Ideally, the HM polyzwitterions will exhibit a unique combination of the stimuli-responsive behaviors observed in previously examined systems.

Another goal of this research is to investigate the interaction of surfactants with the HM polyzwitterions. Surfactants are critical components in micellar enhanced EOR (e.g. polymer-surfactant flooding) processes because of their ability to reduce interfacial tension and mobilize oil trapped in reservoir formations. We aim to synthesize polymer systems that will demonstrate synergistic increases in solution viscosity upon the addition of surfactants. Such polymer systems may demonstrate superior performance as mobility control agents in micellar enhanced EOR processes due to surfactant-induced viscosity enhancement.

This report contains a series of terpolymers containing acrylic acid, methacrylamide and a twin-tailed hydrophobic monomer were synthesized using micellar polymerization methods. These polymer systems were characterized using light scattering, viscometry, and fluorescence methods. Viscosity studies indicate that increasing the nonpolar character of the hydrophobic monomer (longer chain length or twin tailed vs. single tailed) results in enhanced viscosity in aqueous solutions. The effect of surfactants on the polymer systems were also studied. The interactions of these polymers with surfactants were investigated. These surfactants include sodium dodecyl sulfate (SDS), cetyl trimethylammonium bromide (CTAB), Triton X-100. Viscosity measurements of DiC_6AM and DiC_8AM mixtures indicate little interaction with SDS, gelation with CTAB, and hemimicelle formation followed by polymer hydrophobe solubilization with Triton X-100. The $DiC_{10}Am$ terpolymer shows similar interaction behavior with CTAB and Triton X-100. However, the enhanced hydrophobic nature of

the DiC_{10} polymer allows complex formation with SDS as confirmed by surface tensiometry. Fluorescence measurements performed on a dansyl labeled $DiC_{10}Am$ terpolymer in the presence of increasing amounts of each of the surfactant indicate relative interaction strengths to be CTAB>Triton X-100>SDS.

Current research in our laboratories is focused on the use of polymers for mobility control in fluid flow through porous media. When polymers have larger coil hydrodynamic volumes in solution, these solutions offer more resistance to flow through a porous media. This resistance is due to the large solution extensional viscosities possessed by these polymer solutions. Large polymer coil hydrodynamic volumes are formed by high molecular weight macromolecules that are highly solvated by the solvent. The ability of an aqueous solvent to expand a water-soluble polymer's hydrodynamic volume depends upon at the solvent's temperature and the presence of electrolytes in the fluid. Polymer flooding fluids conditions are known to vary as they leave the injection wellhead and thereafter penetrate into an oil reservoir. Thus, it is expected that temperature changes should alter the extensional viscosity and solubility properties of the aqueous polymer solutions used in enhanced oil recovery.

For the above reason, an experimental program has been undertaken to examine polymer solution extensional viscosity properties at elevated temperatures. Our efforts are presently directed at experimentally measuring polymer solution flow properties experiencing fluid extension as fluid temperatures are altered. This data has been analyzed using polymer solution extension rheology theory and compared to theoretical expectations.

In this study a hypothesis was formulated that presumes that polymer coils will extend only when the rate of coil extension is greater than the rate of coil recovery from an extensional strain. A mathematical analysis using this hypothesis was used to develop a relationship that predicts the minimum fluid extension rate that produces coil extension. The minimum fluid extension rate was shown to be inversely proportional to the polymer coil's hydrodynamic diameter. Application of this relationship to limited experimental data shows that the data are consistent with the proposed hypothesis.

This finding implies that in typical reservoir flooding conditions where fluid extension rates are very low, polymer coil extension that decreases displacing fluid mobility and improves oil recovery will occur only if the coil hydrodynamic volume is extremely large. Large coil hydrodynamic diameters are formed when polymer molecular weights are high and the polymer solution intrinsic viscosity is large at the temperature conditions existing in the oil reservoir.

Much of our recent research efforts have also been directed toward modeling dilute polymer solution properties as functions of solution temperature and composition properties. As previously reported we first modeled polymer intrinsic viscosity, a measure of polymer hydrodynamic coil volume, as a function of both polymer molecular weight and solution temperature for neutral polymers in dilute solution. The model was

shown to be consistent with several sets of experimental data for both aqueous and organic solvents.

Since most polymers of interest for enhanced oil recovery are ion-containing and water soluble, we explored a new interpretation of the well-known Odjik-Skolnick-Fixman (OSF) theory to account for the contribution of electrostatic interactions to intrinsic viscosity. As explained in our last report the new model suggested that a universal relationship exists between polyion intrinsic viscosity and the ratio of the Debye-Hückel screening length, a function of solution salt concentration, to the spacing between polyelectrolyte charges. Experimental data, however, tended to form three groups rather than the one expected from theory, with an apparent discrepancy stemming from low versus high molecular weight polymers.

This work has been further extended, and recent improvements are presented in this report. Specifically, Yamakawa-Fujii theory has been applied to estimate the Flory-Fox factor for each polymer-solvent system studied. The calculated factor values for real polymer-solvent systems are somewhat lower than that previously used, the theoretical value for a perfectly random, flexible coil. This modification has eliminated the discrepancy previously reported.

The modified model based on Yamakawa-Fujii and OSF theories was found to describe the contribution of electrostatic forces to the excluded volume of all polyelectrolytes in solution containing sodium chloride. The model appears valid for flexible polymer coils in aqueous salt solutions where intermolecular interactions are minimal. The dimensionless viscosity was related to the dimensionless ratio of solution screening length to polyion charge spacing by a constant. Several sets of experimental data from the literature and from our laboratory have been analyzed according to the model and suggest that the ratio of the two dimensionless groups is a universal constant equal to 2π.

Task 1: Polymer Synthesis

Background

To date, our synthetic research efforts have been focused on the development of stimuli-responsive water-soluble polymers designed for use in enhanced oil recovery (EOR) applications. These model systems are structurally tailored for potential application as viscosifiers and/or mobility control agents for secondary and tertiary EOR methods. The goal of previous synthetic work has been to design novel polymers that exhibit large dilute solution viscosities in the presence of the adverse conditions normally encountered in oil reservoirs (such as high salt concentrations, the presence of multivalent ions, and elevated temperatures). The polymers are also designed to have "triggerable" properties that can be elicited by external stimuli, such as changes in pH and/or salt concentration.

Various zwitterionic polymers have been investigated in our laboratories due to their unique responsiveness to saline media.[1] Unlike polyelectrolytes (PEs), which bear *either* anionic or cationic charges, polyzwitterions (PZs) bear *both* anionic and cationic functionalities. PZs may be categorized as polyampholytes (anionic and cationic charges on *separate* repeat units) or polybetaines (anionic and cationic charges on the *same* repeat unit). In aqueous solution, PEs generally collapse with increasing ionic strength due to the screening of intramolecular repulsions between like charges along the polymer backbone.[2] This phenomenon, known as the polyelectrolyte effect, tends to impair the performance of PEs in applications where the polymers encounter saline media. In contrast to PEs, PZ solutions exhibit an antipolyelectrolyte effect in which the polymer adopts a more expanded conformation with increasing ionic strength.[3] This effect is attributed to the screening of intramolecular attractions between the pendant anionic and cationic moieties along the polymer backbone by the small molecule electrolytes. The increase in hydrodynamic size is also accompanied by an increase in solution viscosity, making PZs ideal candidates for salt-tolerant viscosifiers.

Polyzwitterions containing the sulfonate functionality have been thoroughly studied beginning with the pioneering work of Hart and Timmerman.[4] In that work, zwitterionic monomers were prepared by the reaction of 2-and 4-vinylpyridine with 1,4-butanesultone. Polysulfobetaines are typically insoluble in deionized water and require a relatively high content of hydrophilic comonomer or the addition of a critical concentration of electrolyte to achieve solubility and viscosity enhancement. Polysulfobetaines have also been synthesized from acrylic,[5,6,7,8,9,10,11,12] acrylamido,[13,14] and vinyl imidazolium[15,16,12,17] monomers and more recently polysulfobetaine block copolymers have been reported.[18,19]

Another area of interest in our laboratories is the synthesis of hydrophobically modified (HM) water-soluble polymers via micellar copolymerization and their solution behavior in aqueous media. These hydrophilic copolymers contain small amounts (typically $\leq$ 1 mol%) of hydrophobic comonomers that enable viscosification through intermolecular hydrophobic associations.[20] Often referred to as associative thickeners

(ATs), the HM copolymers exhibit greater thickening efficiency and more complex rheological properties compared to their unmodified counterparts. Several polymer systems investigated by our group have proven to be effective ATs with pH- and shear-responsive behavior.[21,22,23,24,25,26,27] Both the PZs and the ATs that have been the focus of our investigations demonstrate extremely high potential for application in areas such as enhanced oil recovery, drag reduction, coatings, personal care, and cosmetics.

In addition to ATs, hydrophobically modified polymers demonstrating surfactant-like qualities have been the subject of considerable research[28,29,30,31] beginning with the classical studies of Strauss.[32,33,34,35] From the work of many researchers, the nature of hydrophobic associations has been shown to be dictated by many factors including, but not limited to polymer microstructure, [36,37,38,39,40,41] the 'bulkiness' of the hydrophobe,[42,43,44,45] and the chemical composition of the hydrophobe (hydrocarbon vs. fluorocarbon).[46,47]

In order to obtain an understanding of how the rigidity of the polymer backbone affects the hydrophobic associations of a polysoap, we reported the synthesis and solution behavior of a series of hydrophobically modified cationic quaternary ammonium polyelectrolytes.[48] In that work, consistent with other reports,[49,50,51] we demonstrated that the introduction of long hydrophobic side chains along the backbone of cationic quaternary ammonium cyclopolymers can result in the formation of polymeric micelles or polymeric aggregates under specified conditions. However, the structures that were formed did not demonstrate environmental responsiveness that would be required for an ideal remediative polymer.

This report contains a series of terpolymers containing acrylic acid, methacrylamide and a twin-tailed hydrophobic monomer that were synthesized using micellar polymerization methods. These polymer systems were characterized using light scattering, viscometry, and fluorescence methods. Viscosity studies indicate that increasing the nonpolar character of the hydrophobic monomer (longer chain length or twin tailed vs. single tailed) results in enhanced viscosity in aqueous solutions. The effect of surfactants on the polymer systems were also studied.

Experimental

Materials

All chemicals were purchased from Fisher Chemical Company or Sigma-Aldrich Chemical Company at the highest purity available. All surfactant studies were performed with the SigmaUltra type surfactant to prevent the contamination by other surface active agents. VA-044 was purified by recrystallization from methanol. Acrylic acid (AA) was purified by vacuum distillation. The twin-tailed hydrophobic monomers, dihexylacrylamide (DiC_6AM), dioctylacrylamide (DiC_8AM), and didecylacrylamide ($DiC_{10}AM$) were prepared using a procedure similar to that described previously [52-53]. While the Syntheses of didodecylacrylamide ($DiC_{12}AM$), ditetradecylacrylamide ($DiC_{14}AM$), and dihexadecylacrylamide ($DiC_{16}AM$) is described later. All monomers are shown in Figure 1.

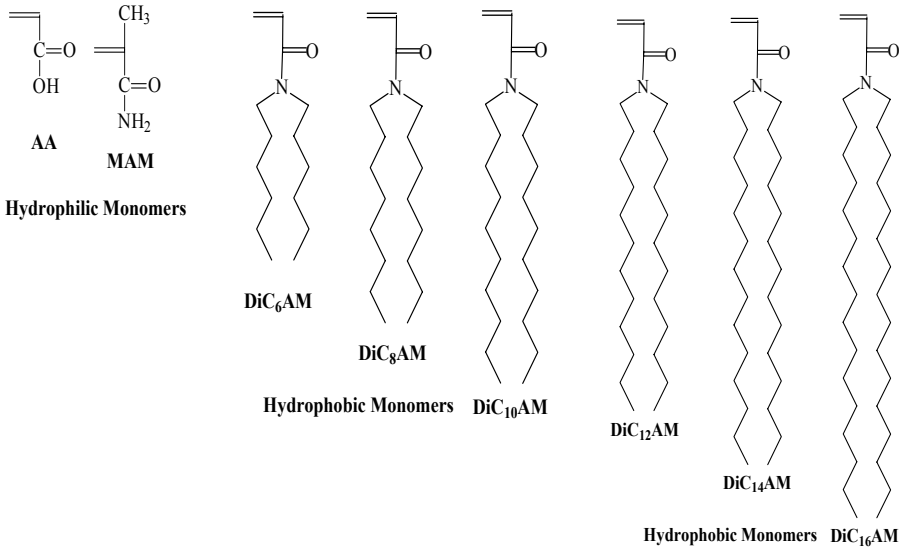

Figure 1. Hydrophilic and Hydrophobic Monomers

Dansyl-2-aminocaprylic acid and succinic acid N-(1-naphthylmethyl) monoamide were chosen as model compounds. The former was purchased from Sigma and was recrystallized from methanol. The nonradiative energy transfer (NRET) donor used for labeling the copolymer backbone was 7-(1-naphthyl-methoxy)-heptylamine and synthesized using the methods of McCormick and Chang.[54] The NRET acceptor, 8-dansyl octylamine, was synthesized as described by Shea et. al.[55] The structures of these chromophores, are shown in Figure 2.

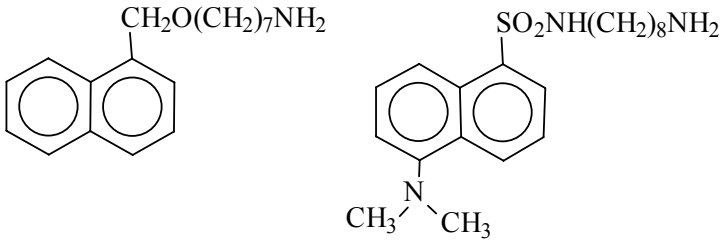

Figure 2. Fluorescence Chromophores Utilized for Fluorescence Energy Transfer Experiments

Monomer Synthesis

Syntheses of N,N-Didodecylamine, N,N-Ditetradecylamine, and N,N-Dihexadecylamine.

Each of the disubstituted amines in the title compounds was synthesized by reacting 0.3 mol of the appropriate N-alkylamine with 0.3 mol of the corresponding N-alkylbromide in 300 mL of acetonitrile in a 500 mL round bottom flask equipped with an overhead stirrer and a condenser. The mixture was heated on a heating mantle and the solution was refluxed for 6 hours. Upon cooling, the resulting amine salt was found to solidify. The salt was filtered, dried, and extracted in methylene chloride using 6M NaOH to deprotonate the salt. The extracted methylene chloride was then concentrated on a rotary evaporator and the resulting diamine was dried *in vacuo* and weighed to give 71, 57, & 52 % yield, and m.p. (salt) 33-34 ^{o}C, 34-36 ^{o}C, 33-37 ^{o}C, respectively. TLC analysis using a chloroform/acetone mixture indicated a single product.

Syntheses of N,N-Didodecyl Acrylamide ($DiC_{12}AM$), N,N-Ditetradecyl Acrylamide ($DiC_{14}AM$), and N,N-Dihexadecyl Acrylamide ($DiC_{16}AM$).

Methylene chloride (100 mL), 0.100 mol of N,N-didodecylamine, N,N-ditetradecylamine, or N,N-dihexadecylamine, and 6N sodium hydroxide (50 mL) were added into a 500 ml 3-neck, round-bottomed flask. The mixture was placed in an ice bath and agitated vigorously using an overhead stirrer under a dry nitrogen atmosphere. When the temperature dropped below 10 ^{o}C, acryloyl chloride (0.104 mol) in methylene chloride (25 ml) was added slowly from an addition funnel such that the temperature was maintained below 10^{o}C. The mixture was stirred for an additional 2 hours after complete addition of acryloyl chloride. The organic layer was then separated in a 500 ml separatory funnel, washed twice with water, once with concentrated NaCl solution, and dried over anhydrous magnesium sulfate. The solvent was removed on a rotary evaporator to yield a light yellow oil (yield 91 %, 82 %,

and 87 % respectively). TLC analysis using a chloroform/acetone mixture confirmed product purity

Polymer Synthesis

Co- and terpolymers were synthesized by micellar polymerization using SDS as the surfactant to solubilize the hydrophobic comonomer and VA-044 as the free-radical initiator. The total monomer concentration was held constant at 0.44 M and the [monomer]/[initiator] ratio at 3000. Also, the hydrophobic monomer content and the surfactant to hydrophobe ratio (SMR) were maintained at 1 mole% and 25, respectively. The reactions were performed for 3-6 hours at 50 ^{0}C. A typical micellar polymerization is shown in Figure 3 for the synthesis of a terpolymer with MAM/AA/DiC_{10}AM at a feed ratio of 49/50/1.

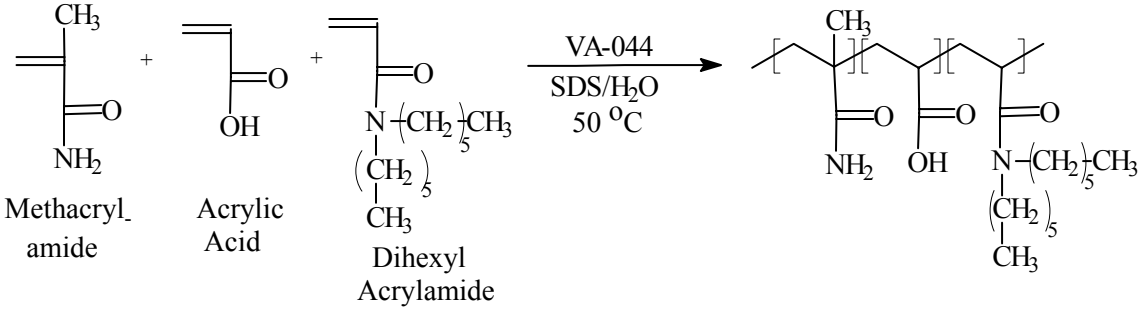

Figure 3. Micellar polymerization of methacrylamide, acrylic acid and dihexyl acrylamide.

In a typical polymerization, deionized water (600 mL) was sparged with N_2 for 30 minutes and SDS (18.0g) was added with stirring under N_2 purge. DiC_6AM (0.592g) was then added with continued stirring for approximately one hour or until the solution cleared. MAM (10.5g1) and AA (8.90g) were then dissolved in the reaction mixture. The pH of the reaction feed was measured and kept below 4.5. To initiate polymerization VA-044 (0.054g) was dissolved in 5 mL of deoxygenated, deionized water and injected into the polymerization vessel. The reaction was allowed to proceed under N_2 for 6 hours after which the terpolymer was precipitated into 1000 mL of methanol. The terpolymer was then washed with fresh methanol and dried overnight in a vacuum oven. Further purification was achieved by redissolving the terpolymer in water and dialyzing for five days against deionized water using Spectra Por No. 4 dialysis tubing with a molecular weight cutoff of 12,000-14,000. The purified polymer samples were then freeze-dried to a constant weight. Synthetic parameters for the terpolymers made in this study appear in Table I.

Table I. Synthetic Parameters Utilized for Twin-Tailed Micellar Polymerizations

Sample	[SDS] mol/L	SMR	MAM (mol %)	AA (mol %)	Hydrophobe (1 mol %)
MAM/AA/DiC_6AM	0.10	25	49.0%	50.0%	DiHexAM
MAM/AA/DiC_8AM	0.10	25	49.0%	50.0%	DiOctAM
MAM/AA/DiC_{10}AM	0.10	25	49.0%	50.0%	DiDecAM
MAM/AA/DiC_{12}AM	0.10	30	49.0%	50.0%	DiC_{12}AM
MAM/AA/DiC_{14}AM	0.10	30	49.0%	50.0%	DiC_{14}AM
MAM/AA/DiC_{16}AM	0.10	30	49.0%	50.0%	DiC_{16}AM

Fluorescence Labeling

The MAM/AA/DiC_{10}AM terpolymer was dissolved in a 70/20 dioxane/formamide mixed solvent system. The appropriate fluorescence label was added to the solution along with the typical DCC/DMAP mixture and the solution was heated to 60 ^{o}C and allowed to react overnight. The details of this reaction are given elsewhere[56]. The resulting solutions were then poured into Spectra Por No. 4 dialysis tubing and allowed to dialyze against deionized water for 15 days. The purified labeled polymer samples were then freeze-dried to a constant weight.

Instrumentation and Analysis

Light Scattering Measurements.

Measurements of dn/dc were performed with a Chromatix KMX-16 Laser Differential Refractometer. MAM/AA terpolymer dn/dc values and molecular weights were determined in 0.5 M NaCl. Dust was removed from samples via centrifugation. Classical light scattering was performed using a Brookhaven Instruments BI-200SM automatic goniometer interfaced to a PC. Using standard Zimm analysis, the molecular weights and radii of gyration were obtained. Prior to analysis all samples were cleaned by centrifuging for 5 mins. All dilution solvents were also cleaned by filtration though 0.45 μm filters to remove dust. Multiple analyses were performed to ensure reproducibility.

Viscosity Measurements.

Viscosity measurements were performed with a Contraves LS-30 rheometer at 25 ^{o}C. All solutions were made at 1.0 g/dl in deionized water and diluted incrementally. Measurements at all concentrations were performed at a constant shear rate of 5.93 sec^{-1} unless otherwise noted. Solution pH values were adjusted with aqueous HCl or NaOH.

Fluorescence Quantum Yield.

Prior to quantum yield determination, the absorbance of the dansyl labels at 330 nm for a polymer concentration of 0.50 g/L was determined. Fluorescence quantum yield was then calculated using equation 1,

$$\Phi_x = \Phi_{st} \frac{A_{st}}{A_x} \frac{I_x}{I_{st}} \frac{n_x^2}{n_{st}^2} \quad (1)$$

in which, Φ is quantum yield, ***A*** is the absorbance at the excitation wavelength, ***I*** is the integral area of the corrected emission spectrum, and ***n*** is the refractive index at the excitation wavelength. The subscript *x* refers to the utilized chromophore and the subscript *st* refers to the standard compound.

Non-Radiative Energy Transfer.

For NRET measurements, an Acton cut-off WG-305 optical filter was used at the excitation wavelength (282 nm) to prevent scattering of the excitation beam from the samples. The dansyl chromophores were excited at 330 nm to observe the dansyl emission spectra. Quantum yields (Φ) of the fluorescent labels were calculated by integrating the areas of the corrected emission spectra in reference to 2-amino pyridine in 0.10N H_2SO_4 as the standard (Φ=0.60 at 282 nm excitation).[57] Quantum yields (Φ) of the dansyl groups excited at 330 nm were calculated by integrating the areas of corrected emission spectra in reference to quinine bisulfate in 1.0 N H_2SO_4 as the standard (Φ = 0.55 at 330 nm excitation).[58] Beer's law corrections were applied for optical density changes at the excitation wavelength. Corrections were also made for refractive index differences.

The Förster distance, r_o has been previously determined to be 23.45 Å for the naphthalene/dansyl donor/acceptor pair, [59] and the NRET quantum efficiency, χ, has been calculated using the method described by Guillet.[60] In this case, the modified Guillet method[19] is used for calculating NRET quantum efficiency, χ, due to the minor absorbance of the dansyl chromophore when 282 nm is used as the excitation wavelength. The modified Guillet equation is given below:

$$\frac{\chi}{1-\chi} = \frac{\Phi_D^0 (I_A - I_A^0)}{\Phi_A^0 I_D} \quad (2)$$

in which Φ_D^0 is the fluorescence emission quantum yield of the donor in the absence of acceptor-labeled polymer excited at 282 nm and Φ_A^0 is the fluorescence emission quantum yield of the acceptor on the acceptor-labeled polymer. I_A and I_D are the integrated emission intensities of donor and acceptor, respectively, in the presence of both donor and acceptor-labeled polymer and I_A^0 is the integrated emission intensity of the acceptor in the absence of donor-labeled polymer.

Steady-State & Dynamic Rheology

The rheological properties of the more viscous polymer solutions were measured with a Rheometrics Scientific SR-5000 controlled-stress rheometer. All measurements were performed at 25 ^{0}C using a cone and plate attachment with a 2^0 angled cone. Steady shear and dynamic measurements were conducted to obtain the steady shear viscosity and the dynamic viscoelastic properties of the studied polymer solutions. To negate any shear history effects, each sample was subjected to a 5 minute preshear of 10 s^{-1} for 5 minutes, followed by a 5 minute rest period prior to measurement. Solution pH values were adjusted using aqueous HCl or NaOH.

Results and Discussion

Monomer Selection, Synthesis, and Characterization.

The major objective of this research was the optimization of the associative thickening efficiency of twin-tailed, hydrophobically modified terpolymers; therefore, selection of the monomers was quite important. Acrylic acid (AA) and methacrylamide (MAM) provide water-solubility and the potential for conformational restrictions (due to the ionizable site in the former and side chain methyl group in the latter) that would be expected to contribute to backbone stiffening. A stiff polymer backbone is an important characteristic for these systems in order to reduce the degree of intrapolymer (closed) association and to help promote interpolymer (open) association. The hydrophobic monomers are a series of twin-tailed acrylamido monomers (Figure 1). DiC_6AM, DiC_8AM, and $DiC_{10}AM$ were synthesized from their corresponding commercially available amines with acryloyl chloride using a Schotten–Baumann procedure[24]. Since the $DiC_{12}AM$, $DiC_{14}AM$, or $DiC_{16}AM$ twin-tailed monomers were not commercially available, we first synthesized the N,N-disubstituted amines and subsequently their corresponding monomers as outlined in the experimental section. Characterization of the hydrophobic monomers was accomplished using ^{1}H NMR, ^{13}C NMR and FT-IR. Details are provided in the experimental section.

Synthesis of Twin-Tailed Associative Polymers

Initial attempts were made to synthesize copolymers consisting of methacrylamide and one mole % of the DiC_6AM, DiC_8AM, or $DiC_{10}AM$ twin-tailed comonomer. Despite high concentrations of SDS, the polymers precipitated shortly after initiation, and the resulting polymers could not be resolubilized in aqueous media. Consequently, terpolymers were synthesized incorporating acrylic acid (AA) to impart pH responsiveness and to promote solubility in aqueous solution at high pH. A typical polymerization scheme is shown in Figure 3. All terpolymers synthesized (Table I) consist of 49 mole % of MAM, 50 mole % of AA, and 1 mole % of the DiC_6AM, DiC_8AM, or $DiC_{10}AM$ twin-tailed hydrophobic monomer.

In the second series shown in Table 1, micellar polymerization of the $DiC_{12}AM$, $DiC_{14}AM$, or $DiC_{16}AM$ twin-tailed monomers with AA and MAM was attempted using

sodium dodecyl sulfate (SDS) as the surfactant. However, SDS, at the concentrations required to make an appropriately microblocky polymer, did not sufficiently solubilize the $DiC_{14}AM$ and $DiC_{16}AM$ monomers. As a result, sodium hexadecyl sulfate (SHdS) was chosen to maintain solubility during the polymerization. A typical polymerization scheme is shown in Figure 3; the compositions of the terpolymers synthesized are summarized in Table I. During polymerization, all polymers remained soluble in the reaction solution. However, after subsequent surfactant removal and purification, the $DiC_{16}AM$ terpolymer was not water-soluble, a characteristic of strong association often observed at high degrees of hydrophobic substitution. While addition of N,N-dimethylacetamide was found to assist in resolubilization in aqueous media, further study of this polymer will not be reported here.

Molecular Weight Determination by Classical Light Scattering

Molecular weights and radii of gyration were determined for each terpolymer. Initially, formamide was chosen due to excellent solubilizing power and the ease of dust removal. Formamide, however, proved not to be a suitable solvent since accurate refractive index increments (dn/dc) could not be measured for these systems. This problem is often encountered in low ionic strength media as documented in earlier reports by Branham and McCormick.[52] Thus, measurements were carried out at 25 ºC in aqueous 0.5 M NaCl (pH 8).

Classical light scattering with the standard Zimm analysis was utilized to determine weight average molecular weight values (M_w) and the mean radii of gyration (R_g) (Table II). For the MAM/AA/DiC_xAM terpolymers, the molecular weights ranged from 0.75 – 1.12 x 10^6 g/mol. Candau et al.[55,61] have determined with N-monoalkyl acrylamide hydrophobic monomers that the polymer molecular weights increase with increasing monomer hydrophobicity due to hydrogen bonding. In our case, since the monomers are disubstituted, no polarity effect on molecular weight is observed.

In the latter set of Table II, classical light scattering with the standard Zimm analysis was utilized to determine weight average molecular weights (M_w) and mean radii of gyration (R_g). The results for those terpolymers which were soluble in 0.5 N NaCl at pH 8 are provided in Table II.

Table II. Molecular Weights and Radii of Gyration for Synthesized Polymers

Sample	**Hydrophobe**	R_G *(nm)*	**MW (g/mol) x 10^{-6}**
MAM/AA/DiC_6AM	DiHexAM	72.3	1.02
MAM/AA/DiC_8AM	DiOctAM	46.2	0.747
MAM/AA/$DiC_{10}AM$	DiDecAM	63.1	1.12
MAM/AA/$DiC_{12}AM$	$DiC_{12}AM$	42.2	0.982
MAM/AA/$DiC_{14}AM$	$DiC_{14}AM$	21.1	0.457
MAM/AA/$DiC_{16}AM$	$DiC_{16}AM$	-	insoluble

Viscometric Studies

Effect of Hydrophobe Length on Solution Viscosity for MAM/AA Terpolymers

Apparent viscosities as a function of concentration in deionized water at pH 8 were determined for the three MAM/AA/DiC_xAM (x = 6, 8, 10) terpolymers as shown in Figure 4. For all three polymers, as the concentration is increased, a sharp increase in the viscosity is observed. This viscosity enhancement results from the formation of hydrophobic interpolymer networks in which the alkyl hydrophobes are associated into micelle-like aggregates. The terpolymer incorporating the DiC_{10} hydrophobe shows the most pronounced increase in viscosity with concentration. Above ~ 0.6 g/dl, the viscosity is beyond the measurable value of the Contraves LS-30 rheometer. Similar trends are observed for the DiC_8 terpolymer which reaches the measurable limit at ~ 0.8 g/dl and the DiC_6 terpolymer which reaches this limit at 0.9 g/dl. Thus, the viscosification efficiency of these three terpolymers closely follows the increasing hydrophobicity of the twin-tailed monomer. The smaller change in the viscosity profile observed in the DiC_8 and the DiC_6 terpolymers as compared to the DiC_{10} terpolymer can be attributed to the lower molecular weight of the DiC_8 terpolymer. This direct correlation of increasing hydrophobe chain length with aqueous solution viscosity is similar to behavior reported by McCormick and Johnson[11,12] for single-tailed, hydrophobically modified polyacrylamides, Jenkins[23-25] for hydrophobically modified alkali soluble/swellable emulsion (HASE) associative thickeners and Schulz et al.[34] for alkylated poly[acrylamide-*co*-sodium acrylates]. As the hydrophobicity of the alkyl substituent is increased, the propensity for interpolymer association and network formation also increases.

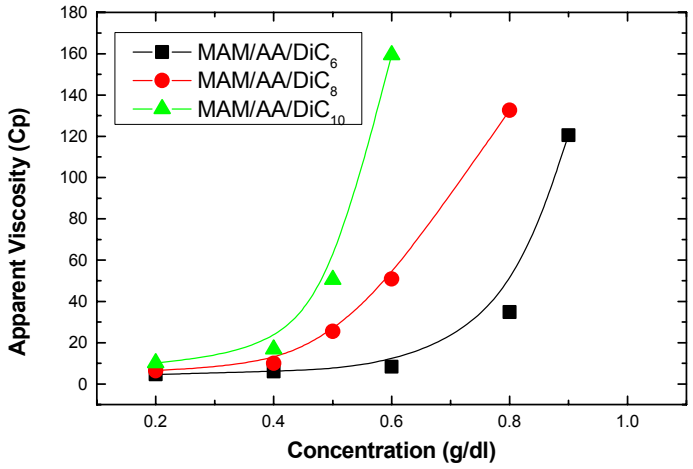

Figure 4. Apparent viscosity dependence on concentration for MAM twin-tailed terpolymers at pH 8.0 and 25 ^oC

Single Tailed vs. Twin Tailed Hydrophobes

The increased viscosification efficiency of the twin-tailed terpolymer as compared to the single-tailed terpolymer is illustrated in Figure 5 for C10 monosubstituted and C10 disubstituted terpolymers. Since the twin-tailed terpolymers have twice the amount of hydrophobe, normalization is necessary for comparison and evaluation of other effects contributing to solution viscosity. From Figure 5 it can be seen that the twin-tailed terpolymer shows dramatically higher increases in viscosity than its single-tailed counterpart. This is likely due to a lower aggregation concentration required for twin-tailed amphiphiles as compared to analogous single-tailed amphiphiles. For mickroblocky N,N-dihexyl acrylamide substituted polyacrylamides, Candau et al.[61] also found the viscosity increase with concentration to be more pronounced in comparison with the corresponding N-hexylacrylamide analog.

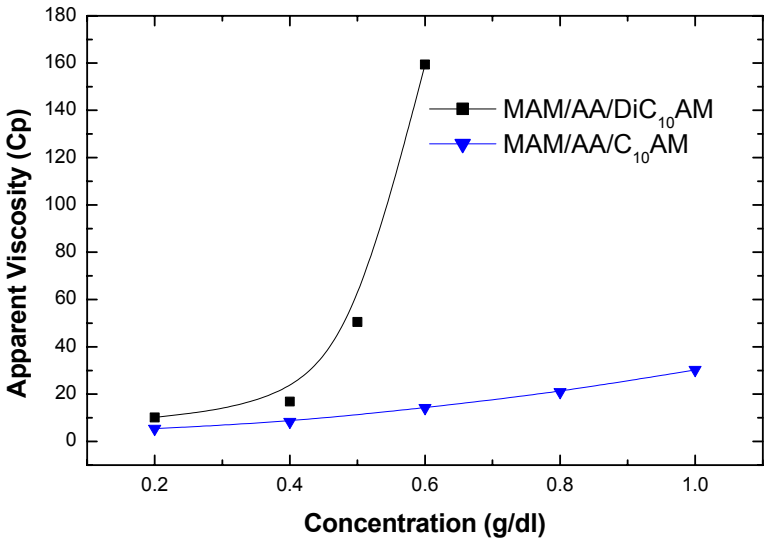

Figure 5. Apparent viscosity dependence on concentration for single and twin-tailed terpolymers at pH 8.0 and 25 ^{o}C normalized for the hydrophobe concentration

Effects of Shear Stress and Hydrophobe Length On Solution Viscosity

Steady shear viscosities (η) as a function of shear stress are shown in Figure 6 for the $DiC_{12}AM$ and the $DiC_{14}Am$ terpolymers at a concentration of 1.0 g/dl and a pH value of 8. Also, shown is the steady shear viscosity for the previously reported $DiC_{10}AM$ terpolymer[53,62]. At these concentrations the polymers are well above their respective overlap concentrations (C*) and exist in highly networked states. As a result all three polymer exhibit high critical yield stresses for network deformation. The shapes of all

three curves are quite similar, although response values differ by decades. At low shear stresses, a small shear-thickening regime is observed. A short plateau region where the viscosity remains relatively constant with increasing shear stress follows at intermediate shear stresses. At higher shear stresses, the samples become shear thinning and exhibit decreases in viscosity characterized by two different slopes. This behavior is characteristic of two distinct changes in the structure of the polymer network occurring at different critical shear stresses, the first being more dramatic than the second. Jenkins et al.[6] have observed similar shear stress profiles for hydrophobically modified alkali-swellable emulsion (HASE) ATs and have attributed the initial more abrupt change to the catastrophic disruption of the polymer network. At the onset of shear thinning, hydrophobic units are in equilibrium between associated and dissociated states. With increasing shear stress in this regime, this equilibrium becomes increasingly shifted to the dissociated state and a dramatic decrease in viscosity is observed. An explanation for the second, structural change is less clear. Under these conditions of shear, the forces placed on the polymer network are such that the interpolymer association equilibrium is shifted almost completely toward the dissociated state.

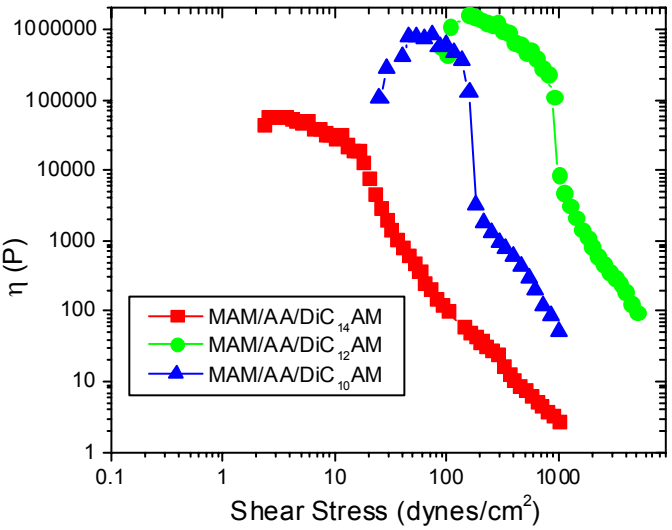

Figure 6. Steady Shear Viscosities (η) as a Function of Shear Stress for $DiC_{10}AM$, $DiC_{12}AM$ and the $DiC_{14}Am$ Terpolymers at a Concentration of 1.0 g/dl at a pH value of 8.0.

In comparing the steady shear viscosity curves for each of the polymers, the effect of twin-tail hydrophobicity on aqueous solution viscosity is readily apparent (Figure 6). The terpolymer incorporating the $DiC_{12}AM$ hydrophobic monomer shows the most pronounced initial viscosity and highest critical stress required to cause network deformation, followed by the terpolymers incorporating the $DiC_{10}AM$ and $DiC_{14}AM$ hydrophobic monomers, respectively. The less desirable behavior of the $DiC_{14}AM$

terpolymer is most likely the result of lower molecular weight and insufficient solubility to promote effective associative thickening. Of the three terpolymers, polymerized under specific conditions outlined in the experimental section, an apparent maximum in AT behavior is reached when the alkyl chain length has a carbon number of 12.

Effect of pH on Viscosity Behavior

Acrylic acid moieties, since they are responsive to pH and ionic strength, can greatly affect conformation of the polymer chain and the resulting hydrodynamic volume in aqueous solutions. In order to evaluate electrostatic interactions, apparent viscosities for the MAM/AA/DiC$_{10}$AM terpolymer at a concentration of 0.1 g/dl were measured as a function of pH (Figure 7). At this concentration (refer to Figure 4) the polymer is in a dilute regime ([η]*[c] < 1) and largely unimeric micelles (closed associations) are expected. In Figure 6 the MAM/AA/DiC$_{10}$AM terpolymer shows an initial decrease in viscosity over the pH range from 4 to 6. This behavior is typical for AA based polymers and results from the partial ionization, leading to hydrogen-bonding between ionized AA moieties and adjacent protonated ones and a subsequent decrease in the unimer hydrodynamic volume[63]. At pH 6, the MAM terpolymer reaches a critical degree of ionization beyond which AA moiety repulsion and chain expansion occur. Finally, around ~ pH 9.5-10, a slight decrease in viscosity is observed due to the high ionic strength of the solution and screening of the charge-charge repulsions. Unlike acrylic acid homopolymers, these systems exhibit a maximum at higher pH values. This is likely a result of the higher degrees of backbone ionization required to disrupt intrapolymer association and effect chain expansion for this highly hydrophobic system.

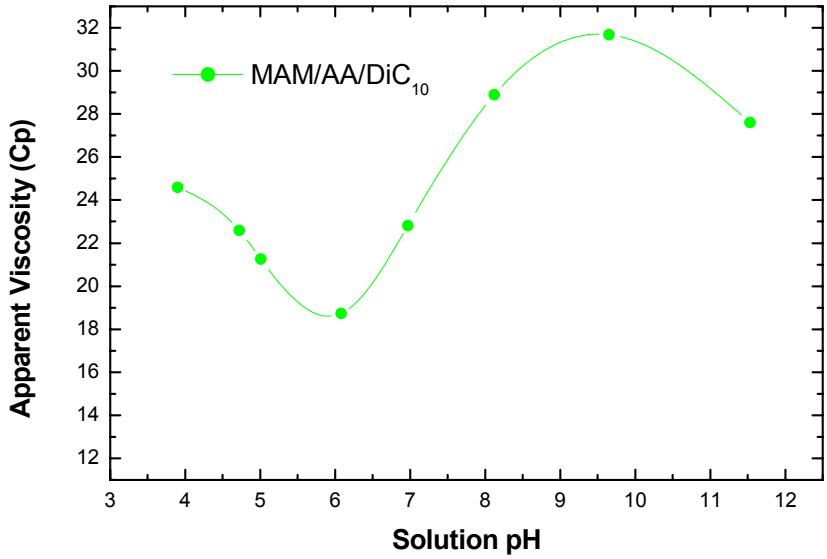

Figure 7. Apparent viscosity vs. pH for the MAM/AA/DiC$_{10}$AM terpolymer at a concentration of 0.1 g/dl.

Incorporation of AA into the terpolymer backbone allows for water-solubility and provides pH responsiveness. In order to investigate the effects of pH on chain expansion of the networked microblocky ATs, the viscosity as a function of pH for both the $DiC_{12}AM$ and $DiC_{14}Am$ terpolymers at a concentration of 0.5 g/dl was examined (Figure 8).

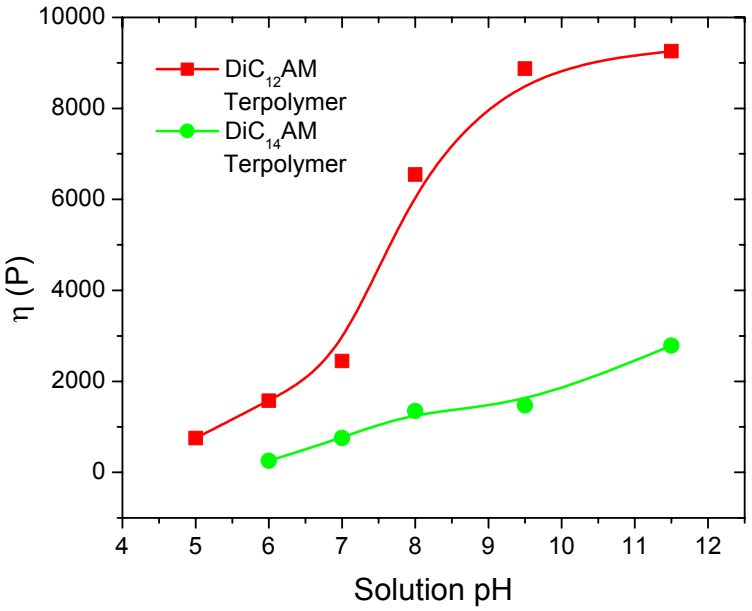

Figure 8. Steady Shear Viscosity vs. pH for $DiC_{12}AM$ and $DiC_{14}Am$ Terpolymers at a Concentration of 0.5 g/dl.

For the $DiC_{12}AM$ terpolymer, a slight increase in viscosity is observed between pH values of 5 and 7. At the lowest pH value, the polymer is only marginally soluble in aqueous solution and likely exists in a collapsed state with most hydrophobes participating in intrapolymer vs interpolymer associates. As the pH is increased over this range (5 to 7), the polymer becomes partially ionized and limited chain (backbone) extension occurs. At pH values between 7 and 11, a larger change in viscosity for the $DiC_{12}AM$ terpolymer is observed. Ionization of the carboxy functional groups into a conformationally extended, energetically favorable state occurs. At these pH values the degrees of ionization are sufficient to overcome hydrophobic forces and disrupt intrapolymer aggregates, resulting in reordered, extended structures with more efficient network formation. The less pronounced behavior of the $DiC_{14}AM$ terpolymer is again likely due to its lower molecular weight and more hydrophobic nature. Solvation and conformational rearrangements with increasing pH are not as favorable. The pH responsive behavior of both terpolymers is illustrated in Figure 9.

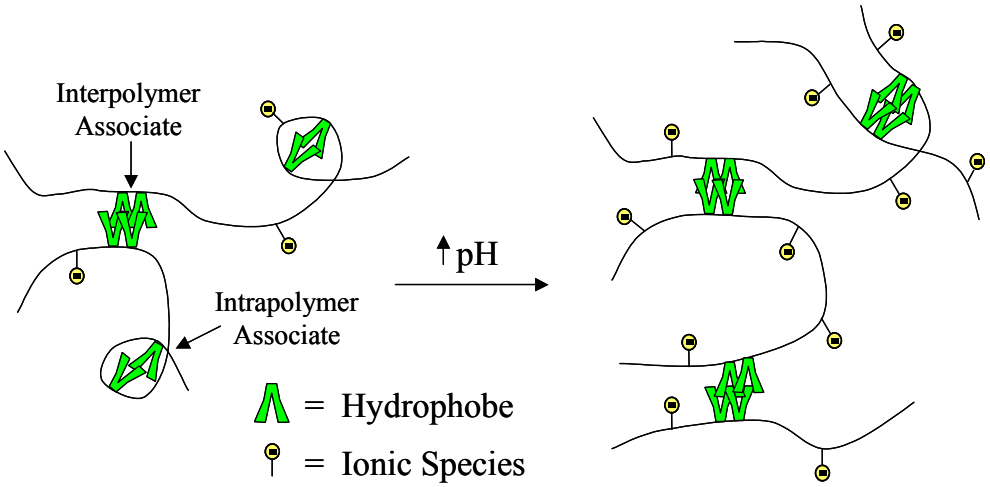

Figure 9. Model Illustrating the Effect of Solution pH on Terpolymer Association Behavior

pH-Responsive Viscoelastic Behavior of Microblocky Twin-Tailed Terpolymer Networks

Dynamic rheology measurements allow the selective probing of chain conformations and/or network states. Experimental data can be fit to an idealized Maxwell viscoelastic model to assess the dynamic behavior of these polymers. Candau et al.[14], have suggested the model to be appropriate for microblocky ATs at intermediate concentrations. In this study, we have examined the pH-dependent behavior of the $DiC_{12}Am$ and the $DiC_{14}Am$ terpolymers at a fixed polymer concentration in order to observe the role that pH plays in their dynamics in solution. The resulting data were fit to a simple Maxwell model which characterizes polymer systems in terms of an elastic (*G'*) and viscous (*G"*) moduli described by equations (3) and (4), respectively

$$G'(\omega) = G_o\omega^2\lambda^2/(1 + \omega^2\lambda^2) \quad (3)$$
$$G''(\omega) = G_o\omega\lambda/(1 + \omega^2\lambda^2) \quad (4)$$

where G_0 is the plateau modulus and λ is the terminal relaxation time at all frequency (ω) values. Thus, *G'(ω)* and *G"(ω)* were determined for the $DiC_{12}Am$ and the $DiC_{14}Am$ terpolymers as functions of ω at selected pH values and fixed polymer concentrations of 0.5 g/dl. Figure 7 represents typical dynamic frequency sweep plots and their fits obtained for the $DiC_{12}Am$ and the $DiC_{14}Am$ terpolymers at pH 7. Experimental *G'(ω) and G''(ω)* data closely follow behavior predicted by the Maxwell model (represented by the dashed line in Figure 10).

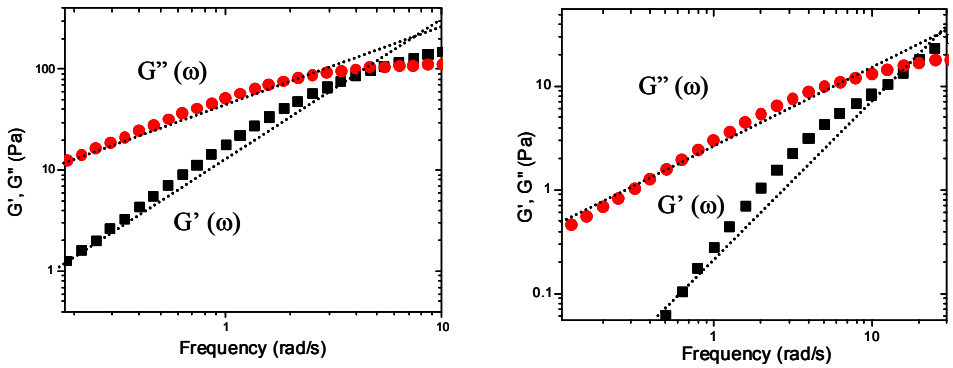

Figure 10. Dynamic Frequency Sweep Study and Subsequent Fitting for the $DiC_{12}AM$ and $DiC_{14}AM$ terpolymers (0.5 g/dl) at pH 7 with τ = 300 & 20 dynes/cm^2, respectively).

From the fit of these data using equations 3 and 4, G_0 and λ at each pH value were determined and are plotted in Figure 11 for the terpolymers studied. Both G_0 and λ exhibit increases with pH for the $DiC_{12}AM$ terpolymer, with small inflections occurring near pH 9 and 7, respectively. The G_0 and λ curves for the $DiC_{14}AM$ terpolymer are similar, showing steady increases with solution pH and small inflections near pH 9.5. Interpretation of these data can be attempted using simple rubbery elasticity theory extended to transient networks by Green and Tobolsky[26]. According to this theory, the magnitude of G_0 is proportional to the number density of mechanically active chains in the network. As mentioned above, network junctions behave transiently with the junctions being in an equilibrium state of disruption and reformation. The lifetime of a junction depends on the residence time of a hydrophobe occupying a space in the junction aggregate. The faster that hydrophobes exit the junction, the shorter this time will be. According to transient network theory, the lifetime of these junctions is directly related to the terminal relaxation time.[26] Thus, the results in Figure 8 indicate that with increasing solution pH, the number density of network junctions increases as does the lifetime of a twin-tailed hydrophobe in a junction. This observation is consistent with a reorganization of network junctions caused by an increase in the solution pH. At lower pH values the network aggregates may be largely intrapolymer in nature. However, as the pH increases and chain expansion occurs, the hydrophobes are able to reorganize and form more effective interpolymer network junctions.

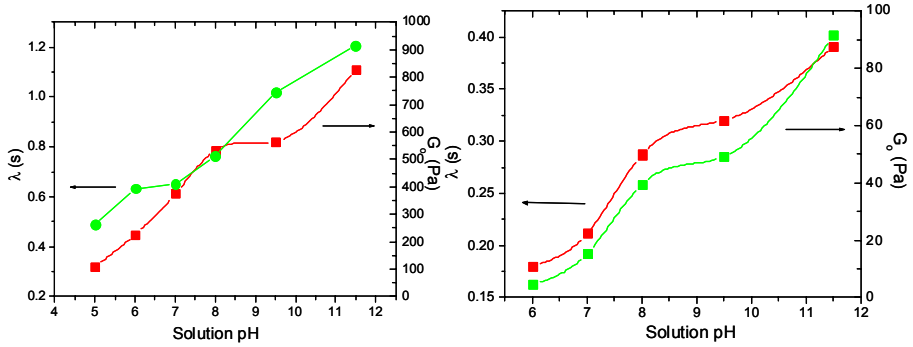

Figure 11. . G_0 and λ as a Function of Solution pH for the $DiC_{12}AM$ and $DiC_{14}AM$ Terpolymers (0.5 g/dl).

Surfactant Interactions

Having established the concentration dependent behavior of the terpolymers in the absence of surfactant, polymer/surfactant interaction was examined using surface tension, viscometric, and fluorescence measurements on selected MAM/AA terpolymers in the presence of an anionic (SDS), a nonionic (Triton X-100), and a cationic (CTAB) surfactant. These surfactants form spherical micelles under the conditions studied. Their critical micelle concentrations are 8.0 x 10^{-3} M, 2.6 x 10^{-4} M, and 9.2 x 10^{-4} M respectively.[23] The structure of these surfactants is given in Figure 12.

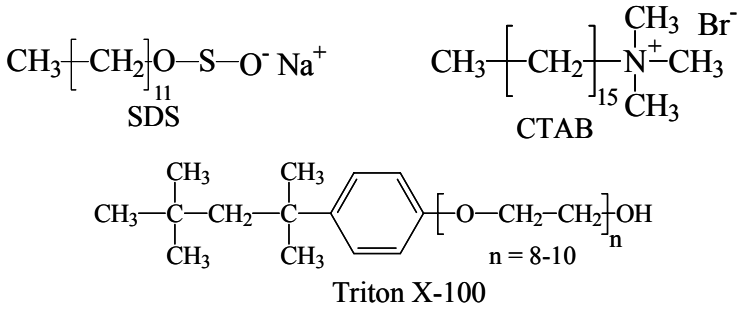

Figure 12. Structures of surfactants SDS, Triton X-100, and CTAB examined for their interaction behavior with twin-tailed associative polymers

Effect of Surfactant Concentration on Polymer/Surfactant Solution Viscosity

Viscosity Measurements on the DiC_6Am and DiC_8Am Terpolymer in the Semi-Dilute Regime

Starting with a concentration of 0.5 g/dl for the DiC_6AM and DiC_8AM terpolymers, surfactant was then added (Figure 13) and viscosity measurements were performed. This concentration was chosen near the onset of association for these two polymers, respectively. For both terpolymers, the addition of increasing amounts of SDS results in a slight decrease in the viscosity of the polymer solution. Since the polymer backbone and the surfactant are similarly charged, no interaction occurs The slight viscosity decrease most likely is due to an increase in the ionic strength of the medium with added SDS. This leads to a lessening of the solvent quality for the hydrophobic polymers as well as a masking of anionic charges, thus decreasing the radii of gyration. Prud'homme has observed similar behavior for the interaction of SDS with sulfonated hydrophobically modified polyacrylamides.[64]

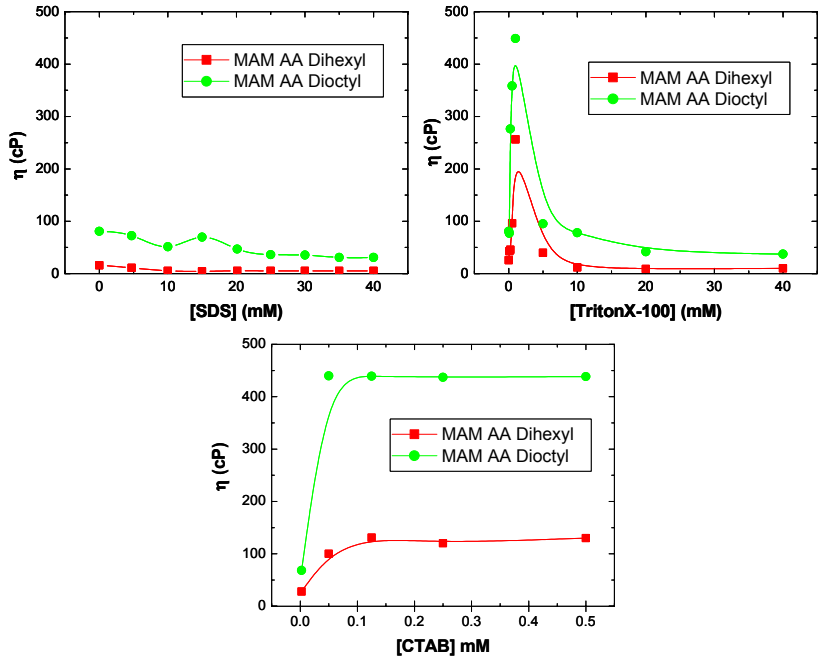

Figure 13. Apparent viscosity measurements as a function of specified surfactant concentration for the DiC_6AM and DiC_8AM terpolymers at concentrations of 0.5 g/dl and pH 8.

As small amounts of Triton X-100 are added, hydrophobic interactions occur with the dihexyl or dioctyl moieties on the polymer backbone, leading to "hemimicelle" formation. Such hemimicelles serve as junction points for interpolymer network formation resulting in pronounced increases in the apparent solution viscosity. Well beyond the CMC of Triton X-100 micelle bridging is disrupted and viscosity decreases to values well below that of the polymer alone. This surfactant concentration dependent behavior is illustrated using a simplified schematic in Figure 14.

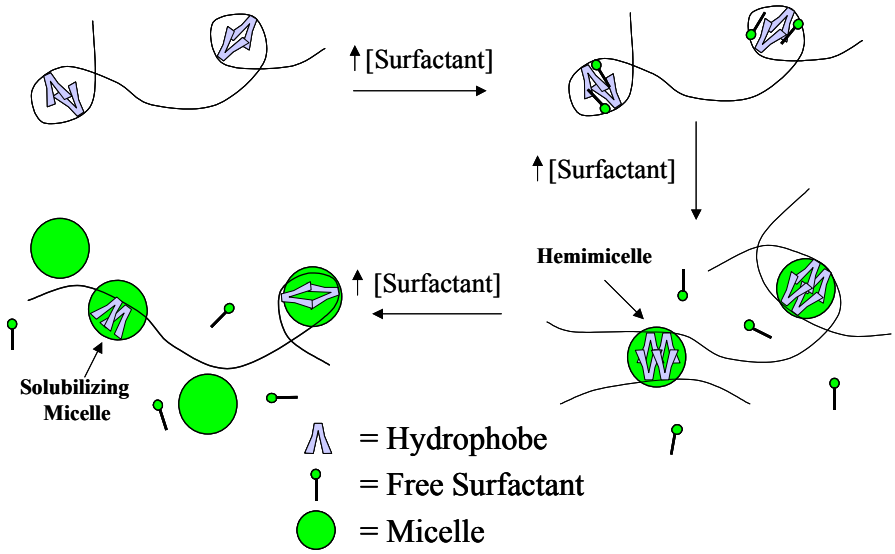

Figure 14. Illustration showing interaction behavior between Triton X-100 and CTAB with the DiC_6Am and DiC_6Am terpolymers at semidilute concentrations

Addition of small amounts of CTAB leads to gelation of both DiC_8 and DiC_{10} polymer solutions. The initial viscosity increase occurs prior to the CMC, indicating a cooperative interaction between the polymer and CTAB with the formation of hemimicelles aided by their interaction with the polymer. Cooperativity, in this instance, results from attractive ionic interactions between the polymer backbone and the surfactant head groups aided by the low local dielectric constant near the hydrophobic microblocks. This behavior results in enhancement of interpolymer association, which is observed macroscopically as gelation. As the CTAB concentration is raised above 0.5 mM, both polymers phase separate. No resolubilization is observed at higher CTAB concentrations probably due to the high charge density of these terpolymers (~ 50 %). Similar behavior has been observed by McCormick and Chang[48] for interaction between a cationic, hydrophobically modified polyacrylamide and SDS.

Viscosity Measurements on the $DiC_{10}Am$ Terpolymer in the Concentrated Regime

The viscosity enhancement observed upon the addition of surfactants to the $DiC_{10}AM$ terpolymer system was too large to be measured using a Contraves LS-30 rheometer; therefore, steady shear measurements were performed with the Rheometrics SR-5000 Controlled Stress Rheometer. All measurements were performed at polymer concentrations of 1.0 g/dl in order to be within the measurement range of the instrument at all surfactant concentrations. At this concentration, the polymer is above C* and associative thickening behavior (interpolymer association) is observed. The results are illustrated in Figure 15. In contrast to the findings for the DiC_8AM and DiC_6AM terpolymers, interaction between the $DiC_{10}AM$ terpolymer and SDS is observed. This is evident from the small enhancement in the in solution viscosity near the CMC of SDS. This behavior is characteristic of the formation of bridging micelles allowing for additional

physical interpolymeric networks. The difference in behavior of this system compared to the DiC_8AM and DiC_6AM systems (essentially no interaction) is a result of the increased hydrophobicity of the DiC_{10} moiety. It is sufficiently hydrophobic to overcome competing ionic repulsion effects, promoting bridging micelle formation. At higher SDS concentrations, a gradual decrease in solution viscosity is observed resulting from solubilization of the existing network hydrophobic junctions by the excess micelles.

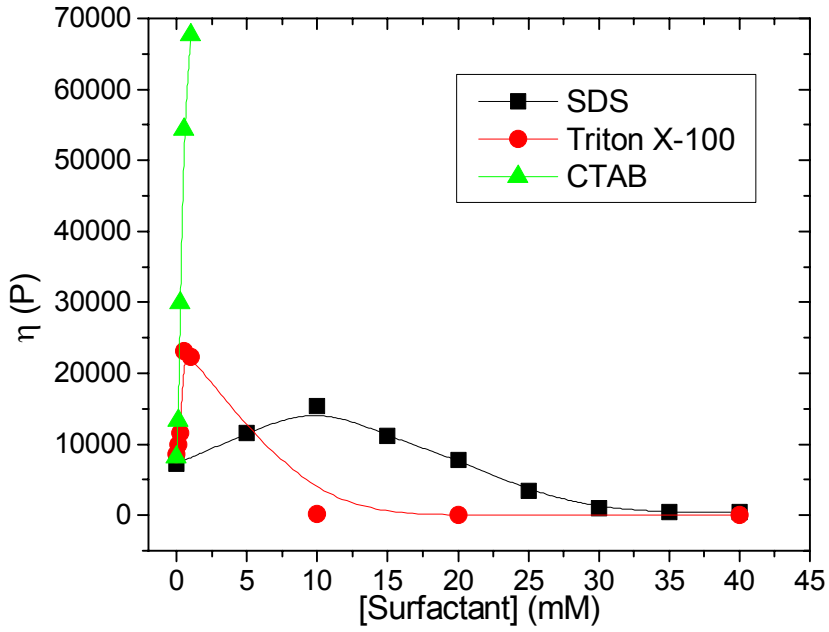

Figure 15. Steady shear viscosity measurements at specified surfactant concentrations for the $DiC_{10}AM$ terpolymer at a concentration of 1 g/dl and shear stress of 20 dynes/cm^2.

Behavior similar to that observed for the DiC_8AM and DiC_6AM terpolymers with Triton X-100 and CTAB was observed for the $DiC_{10}AM$ terpolymer. Like SDS, both surfactants aid in the formation of micellar-bridged crosslinks, though to greater extents. At higher concentrations, Triton X-100 is observed to solubilize the associative microblocks leading to network disruption and viscosity decrease. For the systems containing CTAB at higher concentrations, phase separation occurs. A simplified schematic illustrating the association behavior of these surfactants with the $DiC_{10}Am$ terpolymer network is shown in Figure 16.

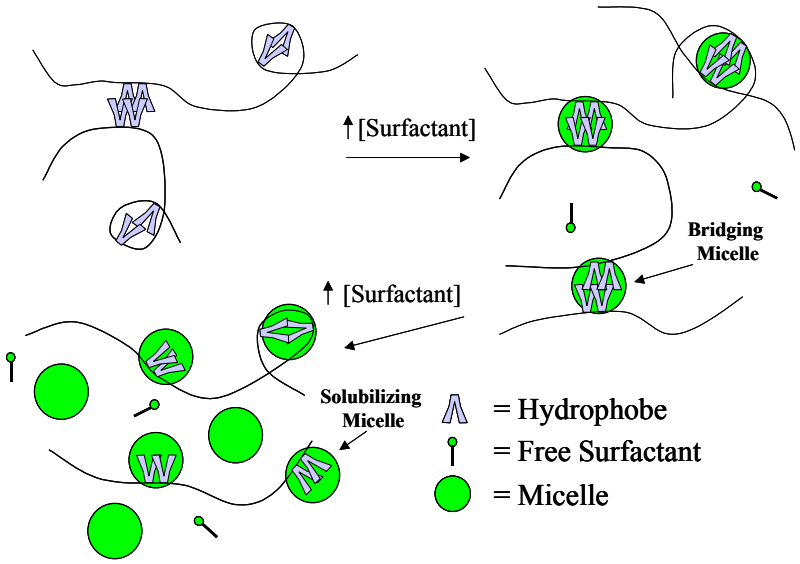

Figure 16. Schematic illustrating interaction behavior between SDS, Triton X-100, and CTAB with the $DiC_{10}Am$ terpolymer interpolymer network.

Polymer/Surfactant Surface Tension Measurements

Surface tension experiments were conducted to further probe the effects of SDS and Triton X-100 on the $DiC_{10}Am$ terpolymer. In order to circumvent any viscous effects imposed by the sample solution, a polymer concentration of 0.05 g/dl was used. At this low concentration, the polymer is in its dilute concentration regime as can been seen from Figure 2. Also, fluorescence energy transfer measurements performed in a previous study indicate that the polymer is in a unimeric state at this concentration. The surface tension curves for SDS and Triton X-100 in the presence and absence of the DiC10Am terpolymer are shown in Figure 17. The surface tension profiles for SDS and Triton X-100 by themselves show typical surfactant behavior. As surfactant is added to water, a small amount dissolves in the bulk solution and the rest orders at the air/water interface. This results in a lowering of the surface tension. At the CMC, the chemical potential of surfactant adsorbed at the air/water interface becomes equal to that required for micelle formation. At this point, excess surfactant is preferentially solubilized as micelles and the surface tension reaches a minimum.

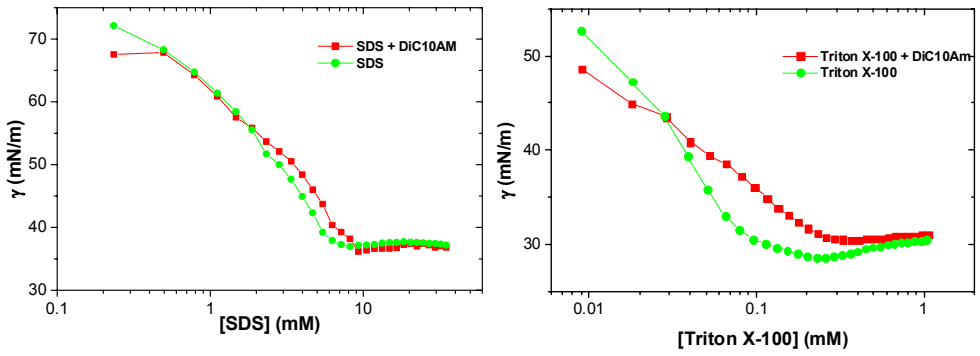

Figure 17. Surface tension measurements for the MAM/AA/$DiC_{10}AM$ terpolymer at a concentration of 0.05 g/dl alone at pH 8 and in the presence of SDS and Triton X-100.

When an interactive polymer is added to the surfactant solution, the surface tension profile changes. Typically, the initial surface tension value for the polymer-surfactant combination is lower than for the surfactant alone. This is especially true if the polymer is surface active, for example the $DiC_{10}Am$ terpolymer being studied here. As described classically by Jones[65] for solutions of SDS and PEO, surfactant initially added to the polymer solution migrates to the air/water interface, lowering the surface tension. At a critical concentration (C_1), also called the critical aggregation concentration or "cac", the chemical potential becomes favorable for the surfactant to interact with the polymer.[66] At a second critical concentration (C_2), all of the polymer sites available for interaction with surfactant become saturated and the chemical potential for the migration of surfactant to the air/water interface is once again favored. This results in further lowering of the surface tension which continues until the CMC for the surfactant is reached. In Figure 16, this behavior is illustrated for the interaction of both surfactants and the $DiC_{10}Am$ terpolymer. Note that Triton X-100 shows much stronger interaction with the polymer than SDS. This is consistent with the steady shear viscosity results shown in Figure 15.

Fluorescence Energy Transfer Measurements

In order to obtain a better understanding of the solution behavior exhibited by twin-tailed, hydrophobically modified acrylic acid polymers on the molecular level, $DiC_{10}Am$ terpolymers (which showed the most pronounced associative thickening tendency) and $DiC_{12}Am$ terpolymers were individually labeled with naphthyl and dansyl chromophores. Mixed solutions containing naphthyl donor and the dansyl acceptor on these separate polymer chains were prepared and nonradiative energy transfer (NRET) measurements were performed following a procedure previously reported by Hu et al.[6] The Förster distance (defined when energy transfer efficiency between chromophore pairs is 50%) for this energy transfer pair has previously been documented to be 23.45 Å. This method is very sensitive for indicating the onset of hydrophobic association and network formation.

Effect of Polymer Concentration on Energy Transfer

$DiC_{10}Am$ Terpolymers

Figure 18 illustrates the emission intensity vs. wavelength behavior for the mixed, individually labeled chains containing the dansyl and naphthyl chromophores (excitation wavelength = 282 nm). As the total polymer concentration is increased, an increase in the emission intensity is observed in the dansyl emission region between 450-580 nm. At 0.01 g/dl and 0.05 g/dl, little emission in this region is observed. Only above concentrations of ~ 0.1 g/dl does significant energy transfer occur. Although evident from direct examination of the emission spectra, a better picture regarding the extent of energy transfer may be obtained by plotting the NRET quantum efficiency as a function of polymer concentration (Figure 19) for the mixed MAM/AA/DiC_{10}AM terpolymers at pH 8.

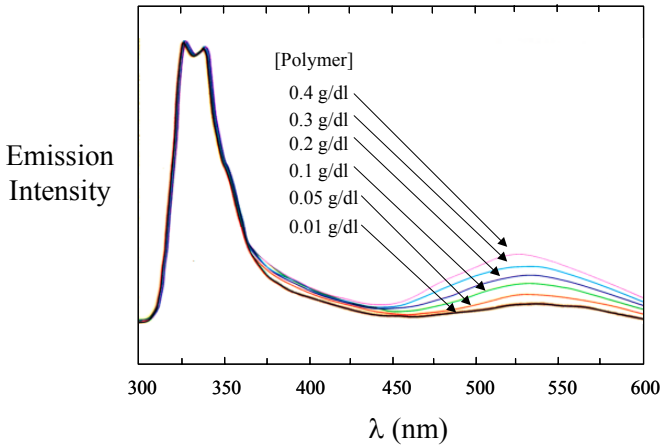

Figure 18

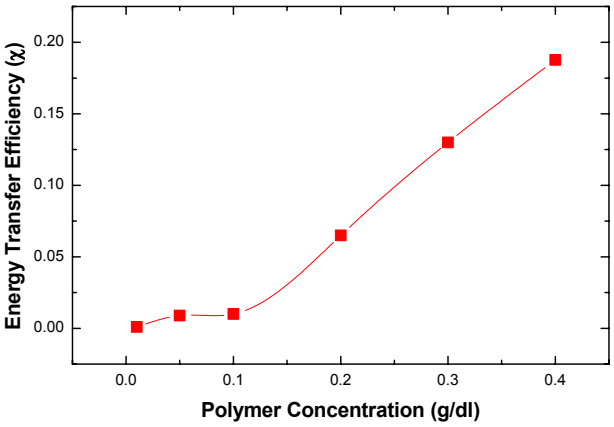

Figure 19

Figure 18. Normalized Emission Spectra for MAM/AA/DiC$_{10}$AM Polymers Excited at 282 nm at pH 8.0

Figure 19. Energy Transfer Efficiency Plot for Two MAM/AA/DiC$_{10}$AM Terpolymers with Naphthalene and Dansyl Labels Mixed in Equimolar Amounts at pH 8.0 and 25 ^{o}C

A significant increase in NRET quantum efficiency occurs at ~0.1 g/dl. This concentration is indicative of initial chain overlap. Below this concentration, most polymer chains likely exist as unimers in solution. Above this concentration, intermolecular association is observed. Kramer and McCormick[5] have observed similar concentration-dependent behavior for labeled poly(acrylamide-co-sodium 11-(acrylamido)undecanoate) polymers. A simplistic model consistent with this behavior is illustrated in Figure 20. The overlap concentration determined by NRET is slightly lower than that determined by viscosity. This behavior is to be expected due to the enhanced sensitivity of fluorescence techniques for determining interchain associations.

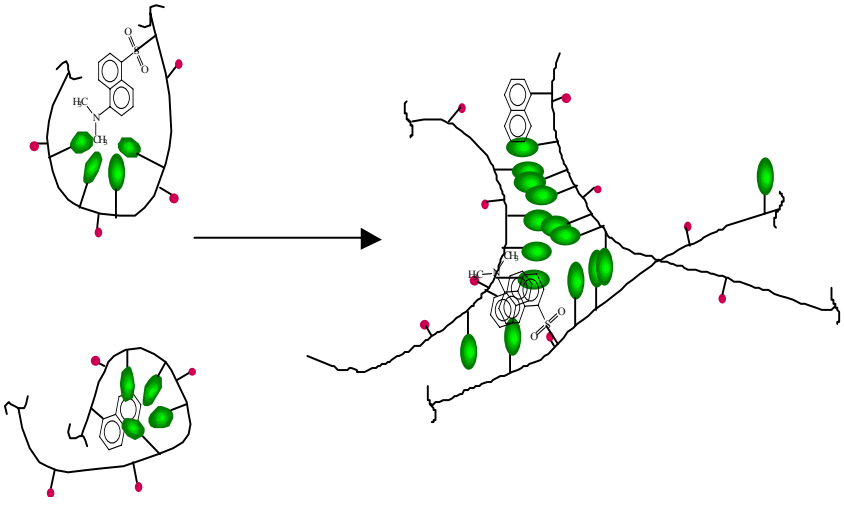

Below C* Above C*

Figure 20. Model illustrating the effect of polymer concentration on nonradiative energy transfer efficiency below and above a critical concentration C*.

DiC$_{12}$Am Terpolymer

Figure 21 illustrates the emission intensity vs. wavelength behavior for the mixed, individually labeled chains containing the dansyl and naphthyl chromophores for five different polymer concentrations when the naphthyl donor was excited at 282 nm. As the total polymer concentration is increased, more naphthyl and dansyl donor and acceptor pairs come within the Förster distance and energy transfer occurs as evidenced by an emission increase in the dansyl region between 450-580 nm. At the lowest polymer concentrations (0.01 g/dl and 0.03 g/dl) little emission in this region is observed. Significant energy transfer begins at a concentration of ~ 0.05 g/dl. While this energy transfer behavior is not readily apparent by examination of the emission spectra, a clearer indication of the amount of energy transferred may be obtained by plotting the NRET quantum efficiency vs. polymer concentration for the mixed labeled DiC$_{12}$AM terpolymer at pH 8. Using the Guillet equation, the NRET quantum efficiency can by calculated at each concentration. This allows for the determination of the microscopic overlap concentration at which labels begin to interact. These data for the DiC$_{12}$AM terpolymer are shown in Figure 22 along with data from the DiC$_{10}$AM terpolymer discussed previously.[24,25]

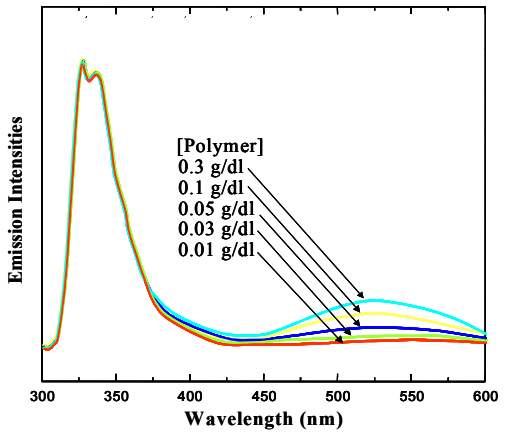

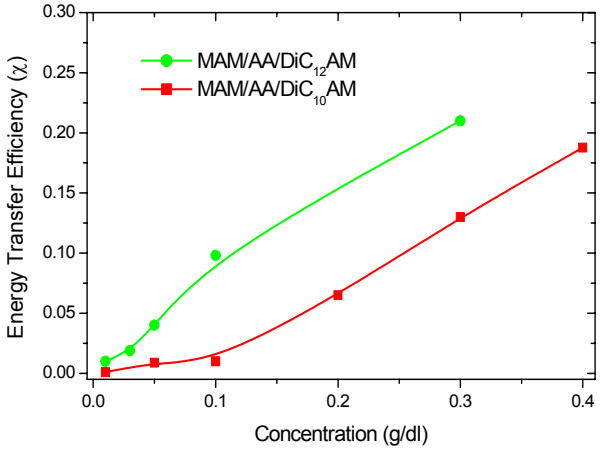

Figure 21

Figure 22

Figure 21. Normalized Emission Spectra for MAM/AA/DiC$_{12}$AM Polymers Excited at 282 nm at pH 8.0 at 25 ^{o}C.

Figure 22. Energy Transfer Efficiency Plot for Labeled MAM/AA/DiC$_{10}$AM & MAM/AA/DiC$_{12}$AM Terpolymers

A large increase in NRET quantum efficiency occurs at ~0.04 g/dl for the $DiC_{12}AM$ terpolymer. Change in the slope at this concentration is indicative of initial chain overlap and the onset of network formation. At concentrations below 0.04 g/dl, most polymer chains likely exist as unimers in solution. The small amount of energy transfer occurring at these concentrations results from the occasional diffusional encounter of chains. Above 0.04 g/dl, interpolymer association occurs and significant energy transfer is observed. A comparison of the $DiC_{12}AM$ terpolymer and the $DiC_{10}AM$ terpolymer previously reported,[23-25] reveals that the onset of intermolecular association occurs at a lower concentration in the former. This behavior is consistent with a model provided for the concentration-dependent association behavior of the $DiC_{10}AM$ terpolymer .

Effect of Solution pH on Energy Transfer

$DiC_{10}AM$ Terpolymers

NRET experiments were also performed on mixed, individually labeled MAM/AA/$DiC_{10}AM$ terpolymers at a fixed concentration of 0.3 g/dl as a function of solution pH. At this concentration, viscosity measurements indicate that the polymer is in the dilute regime, although NRET measurements indicate some interpolymer association occurring at the molecular level. Following corrections for direct excitation, the Guillet equation was utilized to calculate the NRET quantum efficiency at seven pH values between 4 and 10. These data are presented in Figure 23.

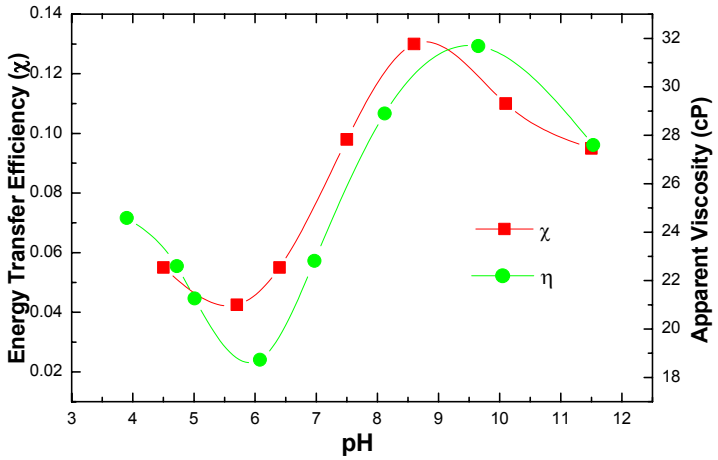

Figure 23. Energy Transfer Efficiency Plot vs. pH for Two MAM/AA/$DiC_{10}AM$ Terpolymer with Naphthalene and Dansyl Labels Mixed in Equimolar Amounts at a Fixed Concentration of 0.3 g/dl.

Although changes in the solution pH are expected to affect the population of reporting dansyl chromophores, calculation of the NRET quantum efficiency based on

quantum yields corrects these data for concentration differences. Between pH values of 4 to 5.5, an initial decrease in viscosity is observed. This behavior is characteristic of AA based polymers and is caused by hydrogen-bonding between partially ionized AA functionalities as discussed above. At pH 5.7, the terpolymer is sufficiently charged such that further ionization leads to chain expansion. Finally, at pH values between 8.5 and 11.5, a small decrease in viscosity is observed due to the high ionic strength of the medium, resulting in charge-charge shielding and a slight collapse in the hydrodynamic volume. Hu and McCormick[6] have observed similar pH responsive behavior for labeled hydrophobically modified poly(sodium maleate -*alt*- ethyl vinyl ether) polymers.

Also plotted in Figure 23 are the viscosity data from Figure 7. While both show the same trends, changes in chain expansion and label interaction indicated by NRET quantum efficiency occur at slightly lower pH values. This once again is believed due to the greater sensitivity of fluorescence methods as compared to rheological methods for indicating changes in labeled polymer chain interactions. The pH responsive behavior of the $DiC_{10}Am$ terpolymer is illustrated in Figure 24.

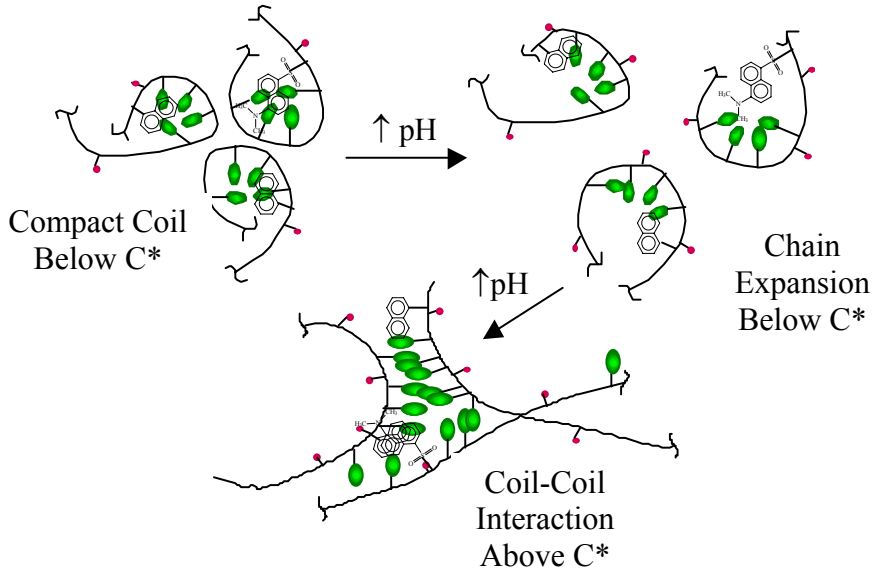

Figure 24. Model Illustrating the Effect of Solution pH on Nonradiative Energy Transfer Efficiency

$DiC_{12}AM$ Terpolymers

In order to verify the effects of solution pH on terpolymer network expansion and dynamics as determined from rheology measurements, NRET experiments were performed on mixed, individually labeled $DiC_{12}AM$ terpolymers at a fixed concentration of 0.1 g/dl as a function of pH. After making corrections for the direct excitation of the dansyl label at 282, the Guillet equation was utilized to calculate the NRET quantum efficiency at six pH values between 5 and 11.5. These data are provided in Figure 25.

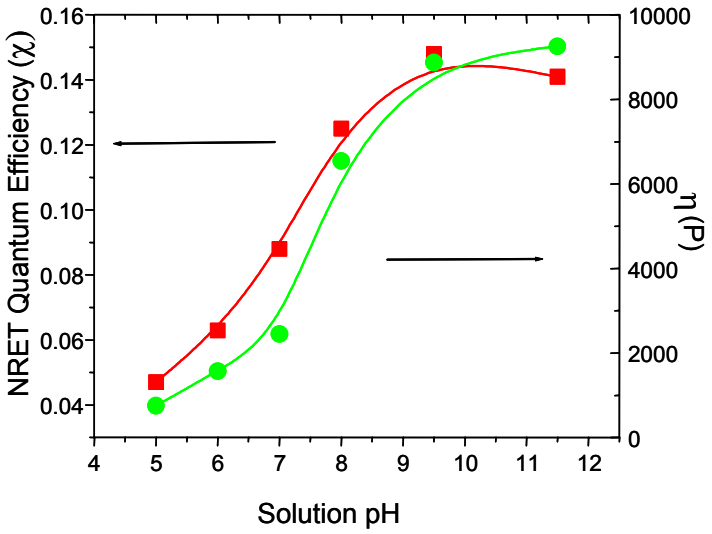

Figure 25. Energy Transfer Efficiency Plot vs. pH for Labeled $DiC_{12}AM$ Terpolymer at a Fixed Concentration of 0.1 g/dl

Close examination reveals that the NRET behavior follows viscosity behavior. A small increase in viscosity is observed between pH values of 5 and 6.5 with an inflection point at approximately 6.5. Due to the high hydrophobicity of the $DiC_{12}Am$ species, the number of intrapolymer associations at these pH values is most likely high. With increasing pH, the polymer becomes increasingly more soluble; however, ionic repulsions at low pH values are not sufficient to cause significant network reorganization. At pH values between 6.5 and 9.5, a large change in NRET is observed. At these higher pH values, ionic repulsion overcomes hydrophobic association at the network junction and the polymers rearrange to form more favorable intermolecular networks. At pH 11.5 a slight decrease in NRET is observed. This is most likely a result of network collapse caused by shielding at high ionic strength. This NRET behavior is similar to that previously observed for a similar $DiC_{10}Am$ terpolymer [67-68] and is consistent with evidence recently reported by Iliopoulos[69-70] showing NMR evidence for both intra- and interpolymer aggregation of hydrophobically modified poly(sodium acrylate) across the entire concentration regime.

Conclusions

MAM/AA terpolymers with twin-tailed hydrophobes exhibit solution properties conducive to associative thickening. Their tendencies toward intermolecular association closely follow the increase in hydrocarbon chain length (hydrophobicity), the terpolymer containing the $DiC_{10}Am$ hydrophobe exhibiting the most pronounced associative thickening. Twin-tailed terpolymers show dramatically higher increases in viscosity than their single-tailed counterparts. This is likely due to the greater hydrophobe density of the twin-tailed monomers which allow enhanced associative junction formation. Energy transfer measurements performed using separately labeled polymers indicate the onset of

association at ~0.1 g/dl for the MAM/AA/DiC_{10}AM terpolymer. This concentration is slightly below that indicated by viscosity measurements. Changes in the energy transfer efficiency as a function of pH at specific concentrations closely follow analogous viscosity behavior. A maxiumum in viscosity and interpolymer interaction is observed between pH values of 8 and 10. At higher pH values, chain collapse occurs due to the high solution ionic strength. At lower pH values, chain collapse results from backbone protonation and an enhancement in intrapolymer hydrophobe association. Thus, it is apparent that the MAM/AA/DiC_{10}Am terpolymer at a pH value between 8 and 10 provides for the most effective thickening of an aqueous solution. In a subsequent paper, systems incorporating higher number hydrophobic, twin-tailed monomers are examined to determine the limits of associative thickening.

The studies performed on twin-tailed associative terpolymers having DiC_6, DiC_8, or DiC_{10} hydrophobic groups, indicated that the greater the hydrophobe chain length, the more pronounced the viscosity enhancement.[68-69] This was attributed to formation of stronger network junctions at lower concentrations by the more hydrophobic microblocks. Solubility problems, however, led us to incorporate comonomers with hydrophilicity and pH-responsiveness. Thus, a series of terpolymers consisting of 49 mol % of MAM, 50 mol % of AA, and 1 mol % of DiC_{12}AM, DiC_{14}AM, or DiC_{16}AM twin-tailed hydrophobic monomer were synthesized to investigate this behavior. The solubility limit was reached with the polymer containing the DiC_{16}AM hydrophobe, even at low concentrations and high pH values. The terpolymer incorporating the DiC_{12}AM hydrophobic monomer exhibited the most pronounced initial viscosity and highest yield stress, followed by the terpolymer incorporating the DiC_{14}AM hydrophobic monomer. The lower viscosity of the latter is thought to be due to higher hydrophobicity and thus closer proximity to the solubility limit.

In regard the effects of surfactant, interaction between twin-tail hydrophobically modified terpolymers and the surfactants SDS, CTAB, and Triton X-100 have been examined. Viscosity measurements performed on the DiC_6AM and DiC_8AM terpolymers indicate no interaction with SDS, gelation with CTAB, and hemimicelle formation followed by disruption for Triton X-100. Similar effects on solution viscosity are also observed for the DiC_{10}Am terpolymer with added cationic and nonionic surfactant. However, a difference is noted for the addition of SDS (anionic surfactant). Some interaction between SDS and the DiC_{10}Am terpolymer is observed to occur. This interaction is a result of the stronger hydrophobic nature of the DiC_{10} hydrophobic tail and is indicative of a shifting from an electrostatically (repulsive) controlled system to a hydrophobically controlled system. These results are supported by surface tension measurements performed on the DiC_{10}AM terpolymer with added SDS which indicate the presence of a critical aggregation concentration for polymer/surfactant interaction.

TASK 5: POLYMER MOBILITY CHARACTERIZATION

SECTION 1. Polyelectrolyte Solution Behavior

Introduction

Aqueous polymer solutions are being studied for Enhanced Oil Recovery (EOR) application because very dilute solutions can significantly decrease flooding fluid mobility in porous media. We have focused on carefully synthesizing model polymers and determining their dilute solution behaviors in controlled fluid flow under select solution conditions. This work has helped to pinpoint parameters that are important to fluid mobility, thereby revealing ways to enhance solution performance in underground applications.

Much of our recent research efforts have been directed toward modeling dilute polymer solution properties as functions of solution component properties and conditions. We first modeled polymer intrinsic viscosity, η_{intr}, as a function of both polymer molecular weight and solution temperature for neutral polymers in dilute solution.[71] The model was shown to be consistent with several sets of experimental data for aqueous and organic solvents.

Since most polymers of interest for EOR are ion-containing, we then explored a new interpretation of well-known Odjik-Skolnick-Fixman (OSF) theory to account for the contribution of electrostatic interactions to intrinsic viscosity.[72] As explained in our last report[72] the model suggested that a universal relationship exists between polyion intrinsic viscosity and the ratio of the Debye-Hückel screening length, L_{screen}, (a function of solution salt concentration) to the spacing between polyelectrolyte charges, b. Experimental data, however, tended to form three groups rather than the one expected from theory, with an apparent discrepancy stemming from low versus high molecular weight polymers.

Finally, another theory was examined in which a polyion coil in solution was modeled as a lightly crosslinked electrostatic gel according to Flory theory.[73] The model was shown to fit all of the applied experimental data. A problem arose though in a lack of physical interpretation for one of the fitted parameters in the model.

Since the modified OSF theory seems to be the most capable of predicting the desired properties, the work has been further extended, and recent improvements are presented here. Specifically, Yamakawa-Fujii theory[75] has been applied to estimate the Flory-Fox factor, Φ, for each polymer-solvent system studied. The calculated Φ values for real systems are somewhat lower than the theoretical value ($\Phi_o = 2.86 \times 10^{23}$) for a perfectly random, flexible coil.

Polyelectrolyte Solution Theory

In previous a report[72] we demonstrated the development of a modified OSF theory. The central modification was in the expression for the electrostatic contribution to the overall polyelectrolyte persistence length in solution, q_e. OSF theory predicted that q_e be expressed as Equation (1), where l_B is the Bjerrum length, for locally stiff polymers. However, this stiff restriction does not apply to EOR polymer systems.

$$q_e = \frac{l_B}{4} \bullet \left(\frac{L_{screen}}{b} \right)^2 \qquad (1)$$

Experimental data for EOR polymer systems of practical interest follow a first order relationship between q_e and L_{screen}/b rather than a quadratic one. Therefore, an empirical expression for q_e was assumed in the form of Equation (2) where k is a constant of proportionality.

$$q_e = k \bullet \frac{l_B}{4} \bullet \left(\frac{L_{screen}}{b} \right) \qquad (2)$$

Substitution of Equation (2) into a relationship derived by Yamakawa[75] for the overall persistence length led to Equation (3), which was the final model for polyelectrolytes in solution containing added low molar mass salt. In Equation (3) η_{intrHS} is the intrinsic viscosity without electrostatic influence (achieved at high added salt concentrations), M is the polymer molecular weight, m_o is the average molecular weight of a monomer unit, and l_m is the length of a monomer unit. The idea was to collect terms which are dependent on the particular polymer-solvent system on the left side of the equation, and to relate them to the ratio of screening length to charge spacing, L_{screen}/b, by a constant of proportionality equal to $(k\, l_B\, \Phi_o^{2/3} / 2)$.

$$\left(\frac{\eta_{intr}^{\frac{2}{3}} - \eta_{intrHS}^{\frac{2}{3}}}{M^{\frac{1}{3}}} \right) \bullet \frac{m_o}{l_m} = \frac{k \bullet l_B \bullet \Phi_o^{\frac{2}{3}}}{2} \bullet \left(\frac{L_{screen}}{b} \right) \qquad (3)$$

As alluded to in our last concluding remarks, Equation (3) is universal under the necessary condition that the Flory-Fox factor, Φ, is constant for all polymer-solvent systems to be modeled. The ideal value of Φ, Φ_o, was theoretically derived by Flory to describe solutions containing perfectly random, flexible polymer coils.[73] Real polymers in solution are not always random, and their departure from the ideal state is amplified as polymer molecular weight and coil flexibility diminish. Because Φ depends on the degree of coil randomness, values of Φ for real, nonrandom systems vary according to

polymer structure and solution conditions. Therefore Φ is not a constant and should be included in the system-dependent left side of Equation (3).

The Bjerrum length in water, l_B, varies slightly with changes in temperature. The variation is negligible, but the dimensions of l_B are such that its inclusion in the left-hand term of Equation (3) renders both sides of the equation dimensionless. Thus, Equation (3) has been rearranged to Equation (4), which relates two dimensionless terms by a constant of proportionality, k/2.

$$\left(\frac{\eta_{intr}^{\frac{2}{3}} - \eta_{intrHS}^{\frac{2}{3}}}{M^{\frac{1}{3}} \bullet \frac{l_m}{m_o} \bullet \Phi^{\frac{2}{3}} \bullet l_B} \right) = \frac{k}{2} \bullet \left(\frac{L_{screen}}{b} \right) \qquad (4)$$

The left side of Equation (4) will be referred to as the dimensionless viscosity, Y, and the ratio L_{screen}/b will be referred to as the dimensionless length, X, so that the equation is of the form $Y = {}^{k}/_{2}\, X$. Data plotted as Y versus X should yield a common line passing through the origin and having a slope equal to k/2.

Equation (4) can be used with data sets consisting of polyion solution intrinsic values measured at either different ionic strengths, hence different L_{screen}, or different charge spacings, b. Given the average polymer molecular structure, the system parameters M, l_m, m_o, L_{screen}, and b can be determined. The method for determining η_{intrHS} was previously described.[78]

In order to determine the value of Φ at each real solution condition, calculations were performed using the Yamakawa-Fujii theory[75]. An iterative routine was employed in which the solution intrinsic viscosity at each condition, along with the theoretical value of the Flory-Fox factor, $\Phi_o = 2.86 \times 10^{23}$, was inserted into Yamakawa's equation relating intrinsic viscosity to polymer persistence length. A persistence length was then calculated and used with the Yamakawa-Fujii algorithm to calculate a new Φ value. The new Φ value was then reinserted into the persistence length equation, and this procedure was repeated until convergence on a value for Φ was reached. The final values of Φ as well as the polymer diameters, D, used in the calculations are reported in Table 1. *(NOTE: We were not able to reproduce Yamakawa and Fujii's tabulated Φ values from their relationship for the case 0.1 < d < 1.0 as printed. In order to obtain the tabulated values, the third term of their coefficient C_3 was changed from $4398.88d^2$ to $43988.8d^2$).*

An important factor in calculations involving polymer persistence length is the distribution of the molecular mass along the polymer backbone. In the above equations this factor is reflected in the ratio of the monomer length to the average monomer molecular weight, l_m/m_o. When determining the average monomer molecular weight of a polyion, it is not obvious whether or not to include the mass of the counterion associated

with a charged monomer unit. Average monomer molecular weights reported in this paper have been estimated by assuming complete counterion retention by up to one half of the total monomer units, and no more.[79,80] (e.g. For a polymer with 30 % of its monomer units bearing a charge, all counterions would be included in the molecular weight. However, if a polyion bears a charge on every monomer unit, only one half of the counterions would be added to the molecular weight.) Due to this new interpretation, some values of m_o have changed from what we previously reported.

Given the information discussed above, experimental data has been plotted in a manner corresponding to Equation (4). All of the literature data plotted in our last report has been included here. The data sets were described and referenced previously.[78,74,76,77] In addition, data collected in our lab for the 10% APTAC copolymer is shown. Experimental data and necessary parameter values are given in Table (III). Polymer acronyms in Table (III) are defined in the nomenclature. A log-log plot of dimensionless viscosity versus dimensionless length for all of the data is shown in Figure (26).

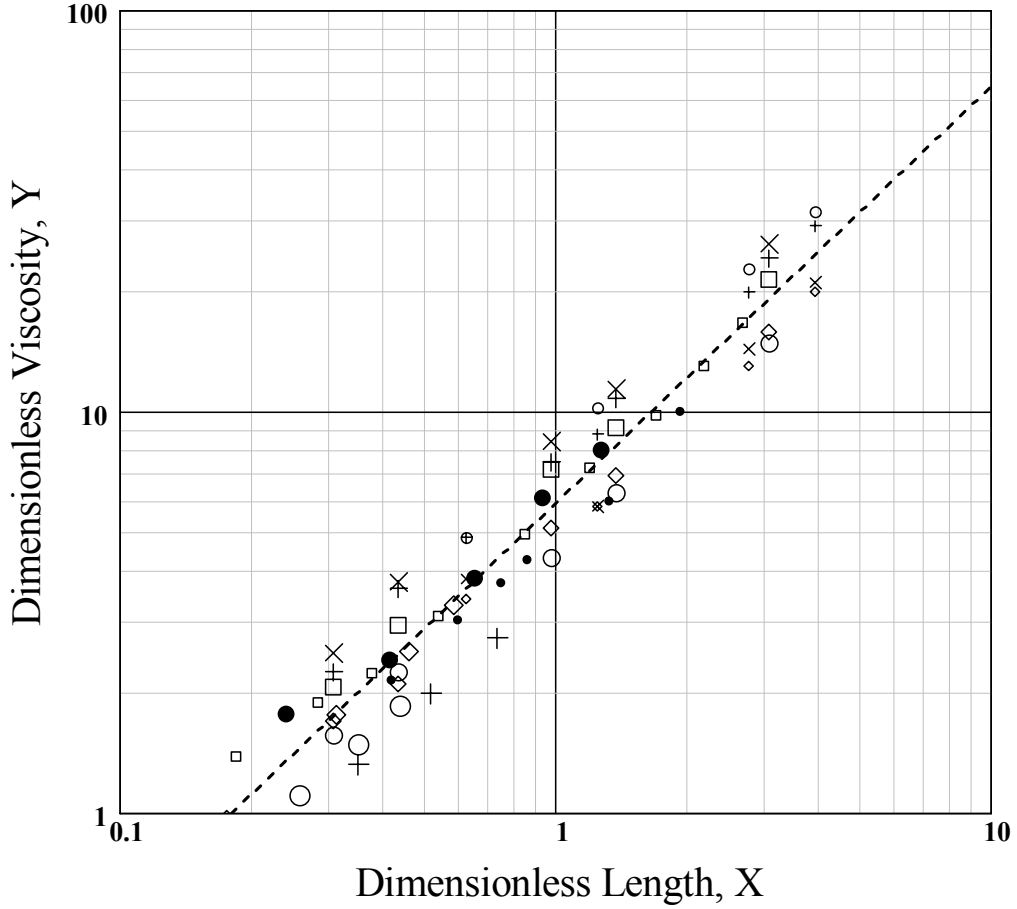

Figure 26. Log-log plot of all data as suggested by Equation (4). Dimensionless viscosity versus dimensionless length yields a universal line with a correlation coefficient equal to 0.9526.

Table III. Experimental Information

Data Set	Parameter							Data			Data(continued)		
	Plot Symbol	T, K	m_o, g/mol	D, Å	$Mx10^{-6}$ g/mol	η_{intrHS}, dL/g	b, Å	I, mol/L	η_{intr}, dL/g	$\Phi x10^{-23}$	I, mol/L	η_{intr}, dL/g	$\Phi x10^{-23}$
NaCMC (a)	○	298	247	14	1.06	7.69	11.0	0.20	11.75	2.27	0.01	27.0	1.81
								0.05	16.3	2.10	0.005	34.8	1.68
NaCMC (b)	+	298	247	14	0.75	6.16	11.0	0.20	9.45	2.18	0.01	19.6	1.75
								0.05	12.1	2.04	0.005	25.8	1.59
NaCMC (c)	◇	298	247	14	0.226	2.90	11.0	0.20	3.95	1.83	0.01	6.68	1.44
								0.05	4.67	1.72	0.005	8.50	1.29
NaCMC (d)	x	298	247	14	0.147	1.89	11.0	0.20	2.74	1.72	0.01	4.80	1.27
								0.05	3.18	1.62	0.005	6.00	1.11
PAA	●	303	72	6	0.48	0.11	7.22	1.02	0.45	2.39	0.24	0.81	2.01
								0.50	0.60	2.22	0.10	1.08	1.79
								0.32	0.72	2.09	0.048	1.70	1.43
AMPS (a)	X	298	218	13	0.86	0.79	9.9	1.0	1.35	2.52	0.05	3.56	2.08
								0.5	1.65	2.43	0.01	7.22	1.63
								0.1	2.79	2.17			
AMPS (b)	+	298	218	13	0.54	0.56	9.9	1.0	0.94	2.50	0.05	2.46	1.95
								0.5	1.18	2.38	0.01	4.79	1.51
								0.1	1.88	2.12			
AMPS (c)	□	298	218	13	0.41	0.42	9.9	1.0	0.71	2.51	0.05	1.75	1.97
								0.5	0.84	2.43	0.01	3.46	1.49
								0.1	1.47	2.09			
AMPS (d)	◇	298	218	13	0.22	0.32	9.9	1.0	0.49	2.39	0.05	1.00	1.87
								0.5	0.53	2.34	0.01	1.77	1.38
								0.1	0.83	2.03			

AMPS (e)	○	298	218	13	0.14	0.19	9.9	1.0	0.30	2.39	0.05	0.63	1.82
								0.5	0.35	2.30	0.01	1.13	1.27
								0.1	0.50	2.04			
APTAC-10	●	298	84.6	7	0.889	1.90	23.4	0.30	3.30	2.35	0.020	7.41	2.55
								0.10	3.85	2.44	0.011	9.35	2.59
								0.041	5.15	2.46			
AM-CMA	□	298	108	9	1.44	2.21	11.4	2.10	3.18	2.68	0.050	8.41	2.40
								0.89	3.58	2.65	0.025	11.19	2.39
								0.50	3.86	2.63	0.015	14.49	2.28
								0.25	4.60	2.58	0.010	18.47	2.16
								0.10	6.25	2.49			
HPAM (a)	＋	303	72.2	6	0.154	0.61	50	0.12	0.83	2.60			
			73.3		0.158		25		1.08	2.48			
			74.5		0.166		17		1.33	2.40			
			75.6		0.167		12		1.59	2.30			
HPAM (b)	○	303	72.2	6	0.381	1.12	50	0.12	1.54	2.64			
			72.7		0.384		34		1.77	2.60			
			73.3		0.389		25		2.00	2.56			
			73.9		0.395		20		2.23	2.52			
HPAM (c)	◇	303	72.2	6	1.14	3.24	50	0.12	4.39	2.63			
			73.1		1.17		28		5.39	2.58			
			74.0		1.20		19		6.38	2.54			
			74.9		1.23		15		7.38	2.50			

Discussion of Results

The modified OSF theory used to develop Equation (4) appears to be consistent with the experimental intrinsic viscosity measurements made using solutions of flexible coil polyelectrolytes in solvents containing a range of sodium chloride salt concentrations. All of the seventy-three data points included here fall on a single straight line within experimental error. The adjustments made to the Flory-Fox factor eliminate the differences in behavior of high versus low molecular weight polymers previously observed.

The slope of the best-fit line shown in Figure (26) has a value of 6.33 with no dimensions. As expected from theory the intercept of the line is near the origin, having a value of -0.48. The correlation coefficient of 0.9526 is remarkable considering the variety of data sources and the sensitivity of the underlying measurements.

A notable observation is that the slope of the linear fit to the data plotted in Figure (26) has a value of 6.33. This value, which is the value of k/2, is virtually equal to 2π, and it follows that k equal 4π. Substitution into Equation (2) yields a new form of the expression for q_e as $q_e = \pi\, l_B (L_{screen}/b)$. Although this relationship was not derived from theoretical principles, the considerable empirical supporting evidence presented here may warrant a theoretical inquiry into its validity.

An important point regarding the theoretical treatment presented in this chapter is that a new dimensionless viscosity is introduced. Its value can be calculated from parameters that are either theoretically known or that can be measured. It is widely agreed that the dimensionless length, $X = L_{screen}/b$, is a determining factor in polyelectrolyte solution properties. A strong correlation exists between the dimensionless viscosity and the dimensionless length that appears to hold for a variety of polymers over a range of solvent conditions. More experimental data is needed to determine whether the correlation is truly universal. Particularly, viscous properties measured for a polyelectrolyte in a non-aqueous solvent having different bulk dielectric properties from water should be investigated.

Conclusion

A new relationship based on Yamakawa-Fujii and OSF theories was developed to describe the contribution of electrostatic forces to the excluded volume of a polyelectrolyte in solution. The model is valid for flexible polymer coils in aqueous salt solutions where intermolecular interactions are minimal. A new dimensionless parameter group termed the dimensionless viscosity was shown to be related to the commonly expressed dimensionless ratio of solution screening length to polyion charge spacing by a constant. Several sets of experimental data from the literature and from our laboratory have been analyzed according to this treatment and suggest that the two dimensionless groups are related by a universal constant equal to 2π. Data for additional polyelectrolyte-solvent systems will be analyzed as it becomes available to test the treatment further.

The theoretical relationship described in this section could prove to be a powerful predictive tool. For a polymer of known molecular structure, only a few viscometric measurements are required to determine the needed parameter values. The theory then allows calculation of polymer solution intrinsic viscosities for a wide range of solution conditions. It has been shown in the past, and new evidence is provided in the following section of this report, that polymer intrinsic viscosity is a strong indicator of solution flow resistance in porous media. Therefore, it is anticipated that the theoretical treatment presented here can be used to predict the solution performance of a particular polymer in a variety of underground conditions.

Nomenclature

Symbol	Description
b	average distance between polyion charges
D	average polymer backbone diameter
k	constant of proportionality
l_B	Bjerrum length
l_m	monomer length
L_{screen}	Debye-Hückel screening length
M	weight average polymer molecular weight
m_o	average monomer molecular weight
q_e	electrostatic persistence length
X	dimensionless length, L_{screen}/b
Y	dimensionless viscosity
Φ	Flory-Fox factor
Φ_o	Ideal value of Φ, 2.86×10^{23}
η_{intr}	polymer solution intrinsic viscosity
η_{intrHS}	polymer solution intrinsic viscosity with no electrostatic forces
NaCMC	sodium carboxymethyl cellulose
PAA	poly(acrylic acid)
AMPS	poly(2-acrylamido-2-methylpropanesulfonate)
APTAC-10	poly(acrylamide-co-3-acrylamidopropyltrimethylammonium)
AM-CMA	poly(acrylamide-co-(N,N,N-trimethyl) amionoethyl chloride)
HPAM	partially hydrolyzed poly(acrylamide)

TASK 5: POLYMER MOBILITY CHARACTERIZATION

SECTION 2. Dilute Polymer Solutions In Extensional Flow

Introduction

Rationale for Experimentation

Current research in our laboratories is focused on the use of polymer additives for fluid mobility control in flow through porous media. Recent observations indicate that larger polymer coil hydrodynamic volumes improve mobility control. Therefore, a good candidate for mobility control in flow through porous media is a high molecular weight polymer that is highly solvated and expanded by the solvent at the applied conditions.

Temperature can affect a polymer solution in many ways. Some polymers in solution at elevated temperatures may chemically degrade. The solubilities of many polymers are altered by temperature changes, and some polymers become insoluble if the solution temperature is elevated or depressed from room conditions. It is well known that temperature also affects the steady shear and dynamic viscosity properties of a polymer solution. Thus, it is expected that temperature changes should alter the extensional viscosity and solubility properties of the aqueous polymer solutions intended for use in enhanced oil recovery.

A Screen Extensional Rheometer (SER) was developed and implemented to simulate fluid flow through porous media and measure fluid extensional viscosity.[82] All previous aqueous polymer solution SER data was collected at room temperature conditions. Because most oil reservoirs are at temperatures greater than room conditions it is important that a knowledge of polymer solution extensional viscosity behavior as a function of temperature be obtained. For this reason, an experimental program has been undertaken to examine polymer solution extensional properties at elevated temperatures.

Our efforts are presently directed at experimentally measuring polymer solution rheological properties experiencing extension over a range of temperatures. This data will be analyzed using polymer solution extension rheology theory and then compared to theoretical expectations.

Background

As explained in previous reports,[82,83] the mobility of a polymer solution flowing through porous media was shown to be a function of the fluid's response to extensional strains. These strains are developed when the fluid velocity varies in the direction of flow. Velocity gradients in the flow direction result from non-uniform size flow channels found within any porous media. Fluid acceleration and deceleration within the pore channels produce the forces that extend and compress the polymer coils found within the solution. Energy is needed to deform the polymer coils as they pass through the porous media and this energy is removed from the flow field causing a decrease in polymer solution mobility.

Polymer solution resistance to extensional flow has been characterized using a Screen Extensional Rheometer (SER).[82] Two parameters to quantify solution extensional rheology have been developed using the SER. These parameters are the fluid flow rate when the polymer coils start to extend, Q_{yield}, and η_c, the polymer coil viscosity. Fluid mobility decreases as the polymer coil viscosity increases.

As described in a previous report,[84] both Q_{yield} and η_c are dependent upon the polymer coil's hydrodynamic volume, V_c. Initial experimentation indicated that when V_c increases, the coil viscosity, η_c, increases and the yield flow rate, Q_{yield}, decreases. To have improved oil recovery when flooding reservoirs with polymer solutions, larger polymer coil hydrodynamic volumes are desired. The change in polymer solution extensional properties with variations in fluid temperature is unknown. This report section investigates this temperature dependence.

Polymer Coil Hydrodynamic Volume

A dilute polymer solution is composed of polymer coils surrounded by solvent. Each coil contains a single polymer molecule and a large amount of associated solvent. A polymer coil's hydrodynamic volume, V_c, is proportional to the product of the polymer's intrinsic viscosity, η_{intr}, and its molecular weight, M, (i.e., $V_c = M\ \eta_{intr.} / N_A$) where N_A is Avogadro's number. Polymer solution intrinsic viscosity can be experimentally determined by measuring the first Newtonian shear viscosities of progressively more dilute polymer solutions. Economics dictate that the polymer solutions used in oil reservoir flooding should have both high molecular weights and large solution intrinsic viscosities which would minimize cost by reducing the polymer concentration needed to achieve adequate reservoir mobility control.

A polymer coil's hydrodynamic volume or intrinsic viscosity depends upon the degree of solvent-polymer thermodynamic interaction. Favorable solvent-polymer thermodynamic interaction increases polymer coil hydrodynamic volume or intrinsic viscosity. When the solvent-polymer interactions are not favorable, the polymer coil volume decreases. When very unfavorable solvent-polymer interactions are present, the polymer coil will completely collapse and will no longer be soluble. Solvent-polymer thermodynamic interaction depends upon polymer molecular structure and concentration, solvent molecular structure, and solution temperature.[85]

Each polymer coil volume can be considered as a sphere having a hydrodynamic diameter, d_h. The coil's hydrodynamic diameter can be found from the polymer coil's hydrodynamic volume according to Equation (1).

$$d_h = \left(\frac{6}{\pi}\right)^{\frac{1}{3}} (V_c)^{\frac{1}{3}} = \left(\frac{6}{\pi}\right)^{\frac{1}{3}} \left(\frac{M\,\eta_{\text{int}\,r}}{N_A}\right)^{\frac{1}{3}} \qquad (1)$$

Dilute Polymer Solutions

A solution's polymer coil volume content can be quantified by using a parameter referred to as the dimensionless concentration, C*. A polymer solution's dimensionless concentration is equal to the product of the polymer mass concentration in the solution, c, and the polymer's intrinsic

viscosity, η_{intr}. Hence, C*, which is the volume fraction of polymer coils within the solution, is given by Equation (2).

$$C^* = c\,\eta_{\text{int}\,r} \qquad (2)$$

In a dilute polymer solution individual polymer coils do not overlap or interact with one another. This condition is met when the volume fraction of polymer coils in the solution is sufficiently less than unity. Each polymer coil in a dilute solution will act independently of other polymer coils, and all coils will respond identically to a given fluid flow condition. Therefore, any excess flow resistance of a dilute polymer solution as compared to the solvent resistance at the same flow rate is due to the sum of the flow resistances produced by each individual polymer coil in the solution. In the work described in this report all polymer solutions have a C* value of 0.1 which has been experimentally shown to give dilute conditions.[86]

Experimental

Previously, the intrinsic viscosity response to changes in solution temperature was experimentally determined for three molecular weight fractions of poly(ethylene oxide) or PEO.[87] Using the intrinsic viscosity values, solutions of these three polymer samples were prepared such that each would have a C* value of 0.1 at the desired experimental temperature. The solvent for all polymer solutions was deionized water. Experimental conditions are reported along with results in Table (1).

The solutions were examined for fluid extensional flow behavior at different solution temperatures. Using the SER, fluid pressure drops across a packed bed were measured for the solvent and polymer solutions (ΔP_o and $\Delta P_{solution}$, respectively) at several volumetric flow rates, Q. As previously reported[82] the data can be plotted according to Equation (3) to find the coil viscosity, η_c, and the flow rate at which the polymer coils extend, Q_{yield}.

$$\left(\Delta P_{solution} - \Delta P_o\right) = \frac{\eta_c}{\beta} Q \qquad when \quad Q \succ Q_{yield} \qquad (3)$$

The left side of Equation (3) will be referred to as the Normalized Solution Resistance (NSR). At flow rates less than Q_{yield} polymer coils do not extend, and the NSR is equal to zero. The β parameter of Equation (3) is a constant that is determined from screen rheometer geometry and other known experimental conditions. β is given by Equation (4). See the nomenclature for an explanation of the parameters used in Equation (4).

$$\beta = \frac{\pi\, D_s^2\, d_{wire}\, f^2}{48\, n\, \varphi\, c\, \eta_{intr}\, (1-f)^2} \qquad (4)$$

Figures 27a, 27b, and 27c are plots of SER data for one molecular weight fraction of PEO (M = $2x10^6$ g/mol) measured at three different temperatures (10, 39, and 75 ºC, respectively). Normalized Solution Resistance is plotted versus volumetric flow rate. Since the shear viscosity of a dilute polymer solution is not measurably greater than that of the solvent, NSR is zero at flow rates less than Q_{yield}. When Q_{yield} is exceeded, however, the polymer coils begin to extend, and the

polymer solution pressure drop becomes greater than the solvent pressure drop (NSR > 0). In the example plots below, Q_{yield} is the flow rate at which the plotted values begin to deviate from zero. Also the slope of the line fit to the data beyond Q_{yield} is proportional to the coil viscosity, η_c, as shown by Equation (3). In Figure (27), increases in temperature induced decreases in polymer intrinsic viscosities from (a) to (b) to (c). These plots illustrate the tendencies of Q_{yield} to increase and η_c to decrease as the intrinsic viscosity or coil volume diminishes.

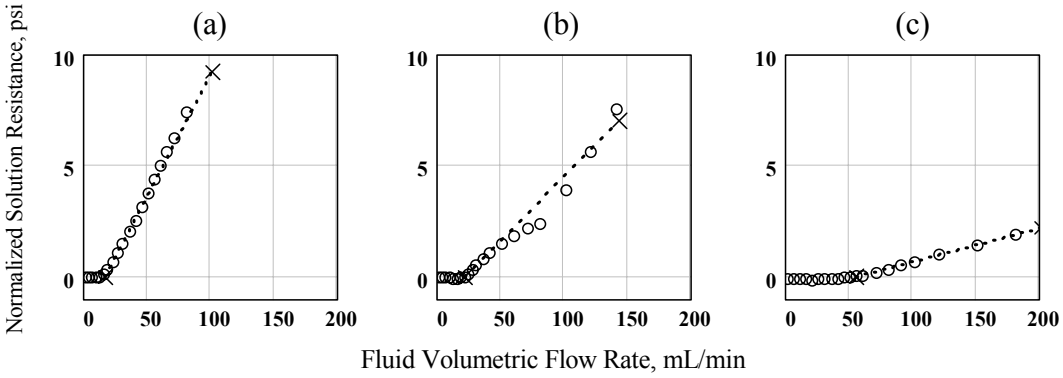

Figure 27. Normalized solution resistance versus volumetric flow rate data from screen extensional rheometer for $2x10^6$ molecular weight PEO. (a) at 10ºC. (b) at 39ºC. (c) at 75ºC.

Explanation of Coil Extension

As discussed in a previous report,[82] the fluid extensional strain rate at which a polymer coil extends, $\dot{\varepsilon}_{yield}$, can be estimated from Screen Extensional Rheometer geometry and the fluid yield flow rate, Q_{yield}, as shown in Equation (5).

$$\dot{\varepsilon}_{yield} \approx \frac{16\, Q_{yield}}{3\,\pi\, D_s^2\, d_{wire}} \frac{1-f}{f} \qquad (5)$$

The fluid extensional strain rate at which polymer coil extension begins may be explained by assuming that coil extension starts when the rate of coil extension, R_E, is equal to the rate of coil recovery from an extensional strain, R_C. If $R_E < R_C$, the polymer coil will not extend because any coil extension developed by the fluid flow field will be instantaneously recovered by the random motions of the macromolecule. Thus, significant coil extension only occurs when $R_E > R_C$.

Coil extension is the result of a difference in fluid drag forces across the polymer coil.[88] This drag force difference increases as both the fluid extension rate and the size of the polymer coil increase. Therefore, the rate of coil extension, R_E, is expected to be proportional to the product of the fluid extensional strain rate, $\dot{\varepsilon}$, and the hydrodynamic diameter of the polymer coil. This relationship is expressed by Equation (6).

$$R_E = k_1 \, d_h \, \dot{\varepsilon} \qquad (6)$$

In Equation (6), k_1 is a proportionality constant and d_h is the polymer coil's hydrodynamic diameter. Equation (1) can be used to determine d_h.

Hassager[89] and Durst[90] have suggested that in dilute solutions the polymer coil recovery rate from a strain deformation would be inversely proportional to the product of the polymer coil's characteristic recovery time, λ_c, and the rate of coil strain deformation, $\dot{\varepsilon}$. Thus, the rate of coil recovery from an extensional strain is given by Equation (7) where k_2 is a proportionality constant and x is an exponent.

$$R_C = \frac{k_2}{\left(\lambda_c \, \dot{\varepsilon}\right)^x} \qquad (7)$$

The coil's characteristic recovery time can be equated to the Zimm response time. This time can be estimated from the polymer's molecular weight, M, and its intrinsic viscosity, η_{intr}.

$$\lambda_c \approx 25 \, M \, \eta_{intr} \, \mu_0 \, / \left(6 \, \pi^2 \, R \, T\right) \qquad (8)$$

In Equation (8), μ_o is the solvent shear viscosity, T is the absolute temperature, and R is the gas law constant. Equation (1) can be used to express Equation (8) in terms of the coil's hydrodynamic diameter, d_h.

$$\lambda_c \approx 25 \, \mu_o \, d_h^3 \, / \left(36 \, \pi \, k_B \, T\right) \qquad (9)$$

where $k_B = R / N_A$ is the Boltzmann constant.

When R_E is set equal to R_C, an equation is formed which can be solved for the fluid extensional strain rate that first produces polymer coil deformation, $\dot{\varepsilon}_{yield}$.

$$\dot{\varepsilon}_{yield} = k_3 \left(d_h\right)^{-\frac{3x+1}{1+x}} \qquad (10)$$

where k_3 is a grouping of several constants, $k_3 = \left(\frac{k_2}{k_1}\right)^{\frac{1}{1+x}} \left(\frac{36 \, \pi \, k_B \, T}{25 \, \mu_0}\right)^{\frac{x}{1+x}}$

Equation (10) can be combined with Equation (5) to find the fluid flow rate that first gives polymer coil extension, Q_{yield}.

$$Q_{yield} = K \, d_h^b \qquad (11)$$

$$\text{where} \quad K = \frac{3\pi k_3 D_s^2 \, d_{wire} f}{16\,(1-f)} \quad \text{and} \quad b = -\frac{3x+1}{1+x}$$

Because all the parameters defining K in Equation (11) were constant in all the polymer solution experiments performed in the Screen Extensional Rheometer, Equation (11) predicts that for any polymer solution Q_{yield} is only a function of the polymer coil's hydrodynamic diameter. Furthermore Equation (11) suggests that a log-log plot of experimentally measured Q_{yield} values versus corresponding polymer coil hydrodynamic diameters should give a straight line relationship in which the straight line intercept, a, and slope, b, are related to x and K, i.e., $K=10^a$ and $x = -(1 + b)/(b + 3)$. It is expected from the work of Hassager[8] that x should have a value of about 1.0 and thus, the b value should be approximately -2.0.

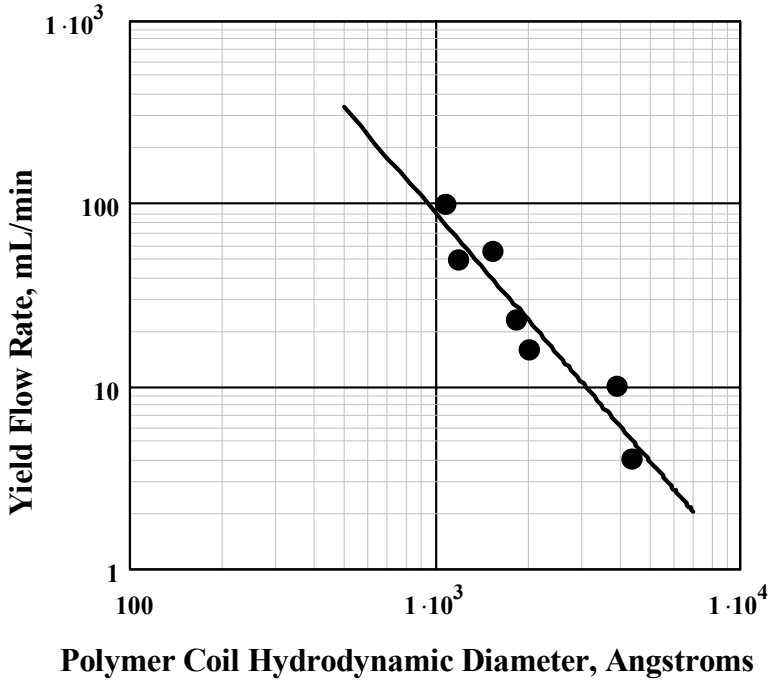

Figure 28: Yield Flow Rate, Q_{yield}, vs. Polymer Hydrodynamic Diameter, d_h

Results

Figure 28 displays a log-log plot of experimental fluid yield flow rates versus polymer coil hydrodynamic diameter to the b power. See Table IV for PEO polymer solution properties and fluid flow conditions. The line drawn in Figure 28 is the fit of Equation (11) to the experimental data. Regression of the experimental data gave a best fit value for b of -1.93 and a K value of 5.54×10^7 mL / (min Angstroms$^{1.93}$). The value for b is only slightly less than that expected from the past work of Hassager[89]. Thus, it appears that a correlation exists as Hassager's work suggests.

Table IV. PEO Experimental Information

Molecular Weight M x 10^{-6}, g/mol	Temperature, K	Intrinsic Viscosity η_{intr}, dL/g	Hydrodynamic Diameter d_h, Å	Yield Flow Rate Q_{yield}, mL/min	Coil Viscosity η_{coil}, poise
0.90	297	5.8	1183	50	0.25
0.90	329	4.2	1058	100	0.05
2.0	283	12.4	1989	16	1.69
2.0	312	9.4	1814	23	0.90
2.0	348	5.5	1517	55	0.24
8.0	297	32	4331	4	3.70
8.0	329	23	3879	10	1.30

The work of Hassager also suggests that, after coil extension, coil viscosity should be related to the polymer coil hydrodynamic volume. Figure (29) shows a plot of experimental coil viscosities versus polymer coil hydrodynamic volume. The plot suggests that the coil viscosity is directly proportional to the hydrodynamic coil volume, V_c. Therefore the function describing the dependence of coil viscosity on coil hydrodynamic diameter is given by Equation (12).

$$\eta_c = k_4 V_c = k_4 \pi d_h^3 / 6 \qquad (12)$$

The slope of the line in Figure (5) gives a k_4 value of 1.90 x 10^{-10} poise/Å.

An explanation for the increase in coil viscosity with coil volume can be rationalized in terms of the large mass of solvent associated with a polymer molecule. During coil extension, stretching of larger volume polymer coils disrupts more solvent contained within the coil than with smaller coils. This disruption of solvent that is in equilibrium with the polymer requires energy. When more energy is required to displace the solvent within a coil, the coil experiences a greater resistance to flow resulting in a greater coil extensional viscosity.

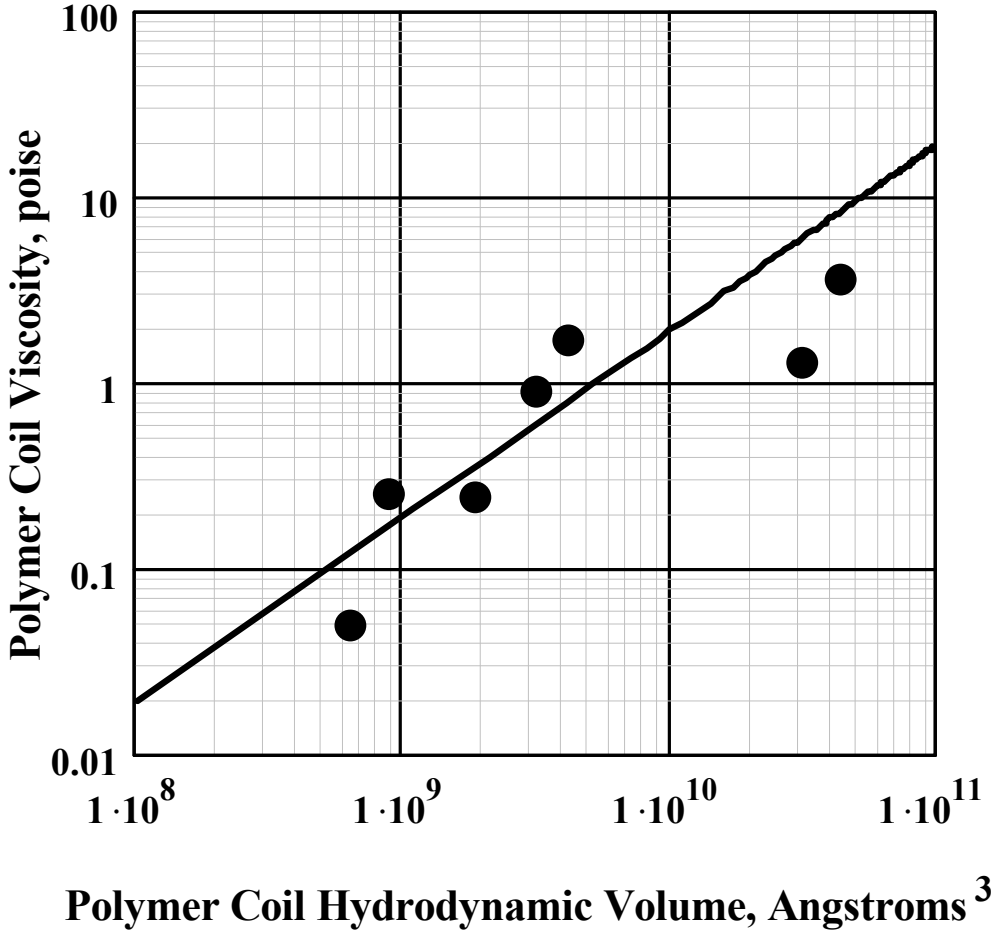

Figure 29: Polymer Coil Viscosity, η_c, vs. Polymer Coil Hydrodynamic Volume, V_c

Conclusion

As a fluid passes through the channels of a porous medium, the fluid is continually accelerating and decelerating. A fluid flowing under these conditions experiences an extensional flow field. The fluid drag forces that are applied to a polymer coil in a fluid under extensional flow are proportional to the average extension rate the fluid experiences. Although the fluid extension rate depends upon the porous medium's channel geometry it always increases, regardless of channel geometry, as the fluid flow rate increases.

If polymer coils in dilute solutions extend and compress as they travel in an extensional fluid flow field they significantly increase the fluid's resistance to flow. However, polymer coil extension and compression will occur only if the extension rate or fluid flow rate through the porous media is larger than some critical value. At the critical flow rate the fluid drag forces applied to a polymer coil are sufficient to extend the coil.

Thus, the critical fluid flow rate for a polymer coil extension is dependent upon polymer chemical structure, macromolecular geometry, solvent - polymer interaction and porous media channel geometry. In general, the critical flow rate value increases as the polymer coil size decreases.

When polymer solutions are used to flood an oil reservoir, very low fluid extension rates exist at large distances away from the injection well-head. To be effective in decreasing displacing fluid mobility during polymer flooding, polymer coils must experience extension as they percolate through the porous media. Polymer coil extension lowers displacing fluid mobility and thereby maintains cohesion to the flood front through the reservoir, and this flooding cohesion increases oil recovery. Thus, an understanding of which fluid flow conditions extend polymer coils is needed to control flooding and improving oil recovery.

In this study a hypothesis was formulated that presumes polymer coils will extend only when the rate of coil extension is greater than the rate of coil recovery from an extensional strain. A mathematical analysis using this hypothesis was used to develop a relationship that predicts the minimum fluid extension rate that produces coil extension. The minimum fluid extension rate was shown to be inversely proportional to the coil's hydrodynamic diameter. Application of this relationship to limited experimental data shows that the data are consistent with the proposed hypothesis.

This finding implies that in typical reservoir flooding where fluid extension rates are very low, polymer coil extension that decreases displacing fluid mobility and improves oil recovery will occur only if the coil hydrodynamic diameter is extremely large. Large coil hydrodynamic diameters are formed when polymer molecular weights are high and the polymer solution intrinsic viscosity is large at the temperature conditions existing in the oil reservoir.

Nomenclature

Symbol	Description
b	exponent, see Equation (11)
C*	dimensionless concentration
c	mass concentration of polymer in a solution
D_s	screen diameter, 1.27 cm
d_h	polymer coil hydrodynamic diameter
d_{wire}	screen wire diameter, 0.0020 cm
f	screen fractional free projected area, 0.16
K	Grouping of constants. Used in Equation (11)
k_B	Boltzmann constant
k_1	proportionality constant in Equation (6)
k_2	proportionality constant in Equation (7)
k_3	grouping of constants, used in Equation (10)
k_4	proportionality constant relating eta {c} to Vc in Equation (12)
M	viscous or weight average polymer molecular weight
N_A	Avogadro's number
n	number of screens connected in series
PEO	poly(ethylene oxide)
Q	fluid volumetric flow rate
Q_{yield}	volumetric flow rate at which polymer coils start to extend
R	gas law constant
R_C	rate of coil recovery
R_E	rate of coil extension
T	absolute temperature
V_c	polymer coil hydrodynamic volume
x	exponent used in Equation (7)
ΔP_o	solvent pressure drop across a porous media
$\Delta P_{solution}$	solution pressure drop across a porous media
ß	grouping of parameters, see Equation (4)

$\dot{\varepsilon}$	fluid extensional strain rate
$\dot{\varepsilon}_{yield}$	fluid extensional strain rate required to force polymer coil extension
η_c	polymer coil extensional viscosity
η_{intr}	polymer intrinsic viscosity
λ_c	polymer coil characteristic recovery time or Zimm response time
μ_o	Newtonian solvent shear viscosity
φ	porosity of screens, 0.52

REFERENCES

[1] Lowe, A. B. and McCormick, C. L. *Chem. Rev.* **2002**, *102*(11), 4177-4189.
[2] Morawetz, H. *Macromolecules in Solution, 2nd Ed*. Robert E. Krieger Publishing Co.: Malabar, FL, 1983, p. 315.
[3] Bekturov, E. A.; Kudaibergenov, S. E.; Rafikov, S. R. *Macromol. Chem. Phys*. **1990**, *C30*, 233.
[4] Hart, R.; Timmerman, D. J. *Polymer Sci.* **1958**, *28*, 638.
[5] Schulz, D. N.; Peiffer, D. G.; Agarwal, P.K.; Larabee, J.; Kaladas, J. J.; Soni, L.; Handwerker, B.; Garner, R. T.; *Polymer* **1986**, *27*, 1734.
[6] Schulz, D. N.; Kitano, K.; Danik, J.A.; Kaladas, J. J. *Polym. Mat. Sci. Eng.* **1987**, *147*-149.
[7] Huglin, M.B.; Radwan, M.A. *Polymer International* **1991**, *26*, 97.
[8] Konack, C.; Rathi, R. C.; Kopeckova, P.; Kopecek, J. *Polymer* **1993**, *34*, 4767.
[9] Konack, C.; Rathi, R. C.; Kopeckova, P.; Kopecek, J. *Macromolecules* **1994**, *27*, 1992.
[10] Monroy Soto, V. M.; Galin, J. C. *Polymer* **1984**, *25*, 121.
[11] Monroy Soto, V. M.; Galin, J. C. *Polymer* **1984**, *25*, 254.
[12] Wielema, T. A., Engberts, Jan B. F. N. *European. Polymer Journal* **1987**, *23*, 947.
[13] Kathmann, E. E.; Davis, D. D.; McCormick, C. L. *Macromolecules* **1994**, *27*, 3156.
[14] Lee, W-F.; Tsai, C-C *Polymer* **1995**, *36*, 357.
[15] Salamone, J. C.; Volksen, W.; Israel, S.C.; Olson, A. P.; Raia, D. C. *Polymer* **1977**, *18*, 1058.
[16] Salamone, J. C.; Volksen, W.; Olson, A. P.; Israel, S.C. *Polymer* **1978**, *19*, 1157.
[17] Wielema, T. A.; Engberts, J. B. F. N. *European Polymer Journal*, **1990**, *26*, 639.
[18] Lowe, A.B., Billingham, N.C., and Armes, S.P. *Macromolecules*, **1999**, *32*, 2141.
[19] Lowe, A.B., Billingham, N.C., and Armes, S.P. *Macromolecules* **1998**, *31*, 5991.
[20] Candau, F. Regalado, E. J.; Selb E. J., *Macromol. Sym.* **2000**, *150*, 241-249.
[21] McCormick, C. L.; Middleton, J. C.; and Grady, C. E. *Polymer* **1992**, *33*, 4184.
[22] Middleton, J. C. *Ph.D. Dissertation*, University of Southern Mississippi, 1990.
[23] Branham, K. D. *Ph.D. Dissertation*, University of Southern Mississippi, 1995.
[24] Branham, K. D.; Snowden, H. S.; McCormick, C. L. *Macromolecules* **1996**, *29*, 254.
[25] Smith, G. L. and McCormick, C. L. *Macromolecules* **2001**, *34*, 918.
[26] Smith, G. L. and McCormick, C. L. *Macromolecules* **2001**, *34*, 5579.
[27] Smith, G. L. and McCormick, C. L. *Langmuir* **2001**, *17*, 1719.
[28] Paleos, M. C. in *Polymerization in Organized Media*; Paleos, M. C., Ed.; Gordon and Breach Science: Philadelphia, **1992**; Chapter 3, 183.
[29] Candau, F.; Zana, R. in *Polymeric Materials Encyclopedia*; Salamone, J. C., Ed.; CRC: Baco Raton, FL, **1996**; Vol. 6, 4287.
[30] Laschewsky, A. *Adv. Polym. Sci*. **1995**, *124*, 1.
[31] Nagai, K. *Trends Polym. Sci*. **1996**, *4*, 122.
[32] Strauss, U. P.; Gershfeld, N. L. *J. Phys. Chem*. **1954**, *5*8, 747.
[33] Dubin, P.; Strauss, U. P. *J. Phys. Chem*. **1970**, *74*, 2842.
[34] Strauss, U.; Vesnaver, G. *J. Phys. Chem*. **1975**, *79*, 1558.
[35] Strauss, U. P.; Schlesinger, M. S. *J. Phys. Chem*. **1978**, *82*, 1627.
[36] Ezzell, S. A.; McCormick, C. L. *Macromolecules* **1992**, *25*, 1881.
[37] Ezzell, S. A.; McCormick, C. L. *Macromolecules* **1992**, *25*, 1887.

[38] McCormick, C. L.; Middleton, J. C.; Cummins, D. F. *Macromolecules* **1992**, *25*, 1201.
[39] Chang, Y.; McCormick, C. L. *Macromolecules* **1993**, *26*, 6121.
[40] Hu, Y.; Smith, G. L.; Richardson, M. F.; McCormick, C. L.; *Macromolecules* **1997**, *30*, 3526.
[41] Hu, Y.; Armentrout, R. S.; McCormick, C. L. *Macromolecules* **1997**, *30*, 3538.
[42] Morishima, Y. *Prog. Polym. Sci.* **1990**, *15*, 949.
[43] Morishima, Y. *Adv. Polym. Sci.* **1992**, *104*, 51.
[44] Morishima, Y. *Trends Polym. Sci*. **1994**, *2*, 31.
[45] Morishima, Y. in *Multidimensional Spectroscopy of Polymers: Vibrational, NMR, and Fluorescence Techniques*; Urban, M. W.; Provder, T., Eds.; ACS Symposium Series 598; American Chemical Society; Washington, DC, **1995**; 490.
[46] Torstensson, M.; Rånby, B.; Hult, A. *Macromolecules* **1990**, *23*, 126.
[47] Stähler, K.; Selb, J.; Barthelemy, P.; Puci, B.; Candau, F. *Langmuir*, **1998**, *14*, 4765.
[48] Chang, Y.; McCormick, C. L. *Polymer* **1994**, *35*, 3503.
[49] Ueda, T.; Harada, S.; Ise, N. *Poly. J.* **1974**, *6*, 473.
[50] Ringsdorf, H.; Schlarb, B.; Venzmer, J. *Agew. Chem. Int. Engl. Ed*. **1988**, *27*, 113.
[51] Butler, G. B.; Do, C. H. in *Water-Soluble Polymers*; Shalaby, S. W., McCormick, C. L., Butler, G. B., Eds.; ACS Symposium Series 467, American Chemical Society, Washington, DC, **1991**, 151.
[52] Branham, K.D., Snowden, S., McCormick, C.L. *Macromolecules* 1996, **29**, 254.
[53] Volpert, E.; Selb, J.; Candau, F.; *Macromolecules*, **1996**, *29*, 1452-1463.
[54] Branham, K.D., Snowden, S., McCormick, C.L. *Macromolecules* 1996, **29**, 254.
[55] Volpert, E.; Selb, J.; Candau, F.; *Macromolecules*, **1996**, *29*, 1452-1463.
[56] Boudreaux, C.J., Bunyard, W.C., and McCormick, C.L. *Journal of Controlled Release*, **1996**, 40, 223.
[57] Rusakowicz, R.; Testa, A. C. *J. Phys. Chem.* **1968**, 72, 2680.
[58] Eastmen, J. W. *Photochem. Photobiol.* **1967**, 6, 55.
[59] Lakowicz, J. R.; Wiczk, W.; Gryczynski, I.; Fishman, M.; Johnson, M. *Macromolecules* **1993**, 26, 349.
[60] Guillet, J. E.; Rendall, W. A. *Macromolecules* **1986**, 19, 224.
[61] Candau, F.; Selb, J.; *Adv. Colloid Intf. Sci.*, **1999**, *79*, 149-172.
[62] Valint, P. L., Bock, J., Schultz, D. N., *Polym. Mater. Sci. Eng*. 1987, **57**, 482.
[63] Hu, Y., Smith, G., Richardon, M.F., McCormick, C.L. *Macromolecules*, **1997**, *30*, 3526.
[64] Panmai, S.; Prud'homme, R. K.; Peiffer, D.G.; *Colloids Surf.,* **1999**, *147*, 3-15.
[65] Jones, M. N. *J. Colloid Interface Sci*. **1967**, *23*, 36.
[66] Mangy, B.; Iliopoulos, I.; Audebert, R.; Piculell, L; Lindman, B. *Prog.Colloid Polym. Sci.* **1992**, *89*, 118.
[67] Smith, G. L.; McCormick, C. L. *Polym. Prepr.* **1998**, *39*, 310-311.
[68] Smith, G. L.; McCormick, C. L. *Polym. Prepr.* **1999**, *40*, 224-225.
[69] Petit-Agnely, F.; Iliopoulos, I.; *J. Phys. Chem. B.,* **1999**, *103*, 4803.
[70] Guillaumont, L.; Bokias, G.; Iliopoulos, I.; *Macromol. Chem. Phys.,* **2000**, *201*, 251.
[71] Rushing, T.S., Hester, R. D., *J. Appl. Polym. Sci*., **2003**, *89(10)*, 2831-2835.
[72] Semi-Annual Report, Stimuli Responsive Polymers, DOE DE-FC26-01BC15317 R03.
[73] Flory, P.J., *Principles of Polymer Chemistry*, Cornell Univ. Press: New York, 1953.
[74] Fevola, Michael, Bridges, J. K., Kellum, M. G., Hester, R. D., McCormick, C. L.,

accepted for publication in *J. Appl. Polym. Sci*, September 2003.
[75] Yamakawa, A.; Fujii, M.; *Macromolecules* **1974**, *7*, 128-135.
[76] Brown, W.; Henley, D.; *Makromol. Chem.* **1964**, *79*, 68-88.
[77] Mabire, F.; Audebert, R.; Quivoron, C.; *Polymer* **1984**, *25*, 1317-1322
[78] Mylonas, Y.; Staikos, G.; Ullner, M.; *Polymer* **1999**, *40*, 6841-6847.
[79] Kulkarni, R. A.; Gundiah, S.; *Makromol. Chem.* **1984**, *185*, 957-967.
[80] Kulkarni, R. A.; Gundiah, S.; *Makromol. Chem.* **1984**, *185*, 969-982.
[81] Fisher, L.W., Sochor, A. R., Tan, J. S., *Macromolecules* **1977**, *10(5)*, 949-954
[82] McCormick, C. L. and R. D. Hester, *Responsive Copolymer for Enhanced Petroleum Recovery, Annual Report,* DOE/BC/15111-1, September, 1999.
[83] McCormick, C. L. and R. D. Hester, *Responsive Copolymer for Enhanced Petroleum Recovery, Annual Report,* DOE/BC/14882-15, February 1996.
[84] McCormick, C. L. and R. D. Hester, *Responsive Copolymer for Enhanced Petroleum Recovery, Annual Report,* DOE/BC/15111-2, February 2001.
[85] Flory, P. J.*, Principles of Polymer Chemistr**y***, Cornell University Press, Ithaca, N. Y. , 1953.
[86] Garner, C. M., *Design and Development of an Instrument for Measuring the Extensional Viscosity of Dilute Polymer Solutions*, Thesis, University of Southern Mississippi, 2000.
[87] McCormick, C. L., and R. D. Hester, *Semiannual Progress Report for Stimuli-Responsive Polymers with Efficiency in Reservoir Recovery Processes*, DE-FC26-01BC15317, September, 2002.
[88] Odell, J. A. and A. Keller, *J. Poly. Sci., Poly. Phys.*, **1986** *B24*, 1889.
[89] Hassager, F., J. *Chem. Phys., 60***, 1974**, 2111.
[90] Durst, F. and R. Hass, *Rheol. Acta.,* **1981**, *20*, 179.